NOTTINGHAM TRENT UNIVERSITY

Voltage Programmable Diffraction Grating Device

MPhil Thesis
(2012)

Wamid (Wham) Al-Shabib

Director of Studies

Prof. Wayne Carleton

Co-supervisor

Dr. Mike Newton

Nottingham Trent University
School of Science and Technology

Acknowledgements

I would like to start by thanking my supervisors at Nottingham Trent University: Professor Wayne Cranton and Dr Mike Newton for all their help and support to submit my work. I would also like to thank the EPSRC. My thanks to Dr Gary Wells and Dr Christophe Tarbi for help, assistance and advice on using experimental techniques and Dr Nicola Day for help in making electrodes for the device, in the clean room. I would like to thank the laboratory technicians Steve Elliott and Dave Parker for their expertise and advice. I would like to thank my wife Katherine Muller and my children Aishah, Aliah and Hamodi (Adam), for their patience during the period of this research.

Abstract

In this research, voltage programmable liquid device has been introduced, studied and a relationship was verified for the electromagnetic relationship between the parameters of the device and the switching application was characterised. The basic operation of the device is to create sinusoidal undulation (wrinkle) on the surface of oil. This wrinkle is used as a variable diffraction grating that changes the wrinkle amplitude in proportion to the applied voltage squared. The device consists of a thin layer (between 8 µm and 50 µm) of 1-Decanol oil which coats a 0.5 µm thick layer of dielectric (SU8 photoresist) that itself has been deposited on to a glass substrate that is patterned with the indium tin oxide electrodes. The pattern of electrodes (interdigitated electrodes) was produced by standard photolithography techniques and the average distance between the electrodes plus the gap between the electrodes (p) that were produced in different devices were 10µm, 20µm, 40µm, 80µm, 160µm, 240µm and 320 µm.

The main area of research was focused on studying the Decanol oil with single frequency 20 kHz squarewave. The square wave voltage V is applied between adjacent electrodes in the interdigitated array such that highly non-uniform electric field profiles are created between the electrodes. The non-uniform electric field create wrinkles (undulation) in the oil surface that is used in the device. That wrinkle is created by dielectrophoresis forces which act to collect the fluid in sinusoidal or nonsinusoidal shape depending on the oil in use. In this research the focus is on oil that produces sinusoidal shape profile.

The static sinusoidal surface wrinkles were recorded and quantified using a Mach-Zehnder interferometer. The amplitude of the wrinkle at the surface of the 1-Decanol has previously been found to follow a V^2 relationship. A theoretical model based on the balance between the increased surface tension of the wrinkled surface and the electrostatic forces predicts this experimentally observed V^2 relationship and also predicts an exponential dependence on the ratio of the amplitude of the sinusoidal wrinkle oil peak to peak is (h) to the distance of the length of the electrodes plus the distance of the gap between the next electrode (p) and that ration is (h/p) of the oil film thickness (h) to the pitch (p). This exponential dependence has been observed experimentally and quantified by observing first the linear relationship between the V^2 and the height of the oil wrinkle on the surface, from this relationship and average height is passed to the theoretical model to scale the derived theoretical relationship to the experimental results. The research examined the diffraction efficiency of zero, first and second orders and was experimentally verified to the theory. The research looked into the use of the wrinkle in the surface as an optical switch, and those experiments are called the dynamic studies. The research looked into the future application of this device and ways to continue the research in this field.

Contents

List of Figures

Chapter 1 Introduction

1.1 Introduction

There has been an increasing demand for photonics devices that can change the direction of laser light, split the laser light to different beams, vary the intensity of the laser light and modulate the laser light with different material properties which the laser light encounters. There are a huge number of photonics devices that can be used in different applications and in a wide variety of sciences from Telecommunications (Lee 2004) , (Lowans 1994), Spectrometers (Heikkila 2008), (Cui 2010), Displays (Senturia 2005), (Jie 2009), Bioscience (Gang 2010), LAB on Chip (Kaler 2010), and sensors (Liscidini, 2009). This increase in demand in the above applications has resulted in the development of different types of instruments and resulted in the demand for small sizes, high switching speed and low cost.

All this development has been made possible with the advances in using different basic physics concepts which have led to different types of photonics devices. The photonic device may be grouped into four types of technologies, Micro-Opto-Electro-Mechanical technology (MEMS), Liquid Crystal (LC) technology, Microfluidic technology and a hybrid group of technologies which cross over between those technologies. The MEMS based technology has proved to have a high scanning speed, low power consumption and it is used in high speed scanning (Yu Du 2009) such as automotive head-up displays, head-worn displays and other mobile computing and personal electronics devices. The disadvantages of MEMS are that it uses a thin mirror plate that mechanically operated and this affects the long term reliability and performance of the photonic device.

Liquid Crystal (LC) technology has moved a great distance and has advanced, especially in the display technology (Scheffer 1984) from mobile phone to large displays, communications (Tocnaye 2004), (Crossland 2004), sensors, beam steering (Tanone 1994) and various research is still advancing in this sector.

The Microfluidic photonics group of devices is an emerging technology which deals with minute amounts of liquid, and can be further classified into three types as Molecular technology (Ferrini 2008), Electrowettings technologies, and dielectrophoresis technology.

Molecular technology is an extremely difficult process, which requires manual manipulation of molecules using such devices as a scanning tunnelling microscope, and Atomic Force Microscopy (AFM). It is an emerging field of technology which promises large optical cross-sections and a short response time, large nonlinear optical responses, energy and charge transport, together with mechanical qualities (film formation, deposition, high damage threshold, low cost technology) (Yoshimura 2011).

The electrowetting technology is currently used in many applications, one of which has gained success for use in large display devices (Heikenfeld and Steckl 2005). It can manipulate up to nano drops of fluid to form the digital pixel on the display (Philips news 2004). The colours used are cyan, magenta and yellow, creating a so-called subtractive colour-mixing system comparable to that used in the printing industry. Moreover, in contrast to Liquid Crystal Display (LCD), no polarisers are needed resulting in a further factor of two gain in brightness. Electrowetting has

proven to be one of the most effective technologies for fast, micro-level control of fluid motion (Vamsee 2009) and is rapidly finding application in a host of areas including the biomedical field, micro pumps and variable-focus lenses. Philips' electronic paper is one further example of this novel technology that is expected to find application in digital camcorders.

A new type of microfluidic photonics approach is being developed in this research project. The device is based on liquid dielectrophoresis, which has been created using a thin layer of liquid coated on an array of interdigitated co-planar strip electrodes (Wells 2009). Dielectrophoresis forces can be manipulated to produce a static sinusoidal wrinkle at the oil-air interface. The amplitude of the wrinkle has a relationship with the applied voltage squared. The fourth group of technology is the hybrid technology like acousto-optic modulator, the hybrid principle of this type technology is illustrated in section 1.9, equation 8.

The novel approach of the dielectrophoresis technology will be described in chapter 2 using the concepts of physics described in this chapter. Chapter 2 describes its operation and the experimental characterisation. Chapter 3 will show the results of the characterisations of this device under static and dynamic experimental setups, and chapter 4 will look at the conclusions and further developments. The remaining sections of Chapter 1 will look at the physics of the device that composes of interdigitated electrodes of different length electrodes and a gap with the same length with oil and voltage supply to create a non-uniform field to create amplitude (wrinkle) in the surface of the oil. This chapter will also describe the tools which have been

used to analyse the static measurements and the theory which the dynamic experiments are based upon.

1.2 Refractive index

The refractive index (n) of material is a number which relates to the variation of the speed of light in that material. It is the ratio of the velocity of light inside a vacuum (c) compared to the speed of light (v) inside the medium.

$$n = \frac{c}{v} \qquad \text{Equation 1}$$

where c is the speed of light (3×10^8 ms^{-1})

The refractive index is frequently found to depend upon the wavelength of light in a given medium. The value of n varies with the wavelength of laser light except in a vacuum, and for a wavelength 589 nm the index of refraction values vary between 1 for vacuum, 1.44 for Decanol oil at 0.1 MHz and 1.58 for normal glass. The refractive index is used in many photonic devices from simple lenses to modern electrowetting optics (Heikenfeld 2008), optical communications, sensors (McCamley 2009), beam steering (Wei 2010), Interferometry (Lee 2009) to create a phase shift between different path lengths.

Refractive index changes are used to create a phase difference between two waves which are initially in phase. As soon as a wave travels to an optically higher refractive index medium the wave slows its speed and this will create a phase shift with the other wave which did not pass through this medium. This change will create

another Optical Path Length (OPL) which is related to the distance travelled times the refractive index of the material.

1.3 Dielectric constant

Dielectric material or the permittivity of an insulating is ε; the permittivity of a vacuum, is symbolized ε_0; and their ratio $\varepsilon/\varepsilon_0$ (ε_r), is called the dielectric constant. Dielectric materials do not possess carriers of free charge which can move about under external control. The charges are bound to the atoms or molecules. Dielectric materials are used to form a capacitor to store charges. ε_r is a constant which represents the increase in the capacitance between two conductors compared to the vacuum space between the two conductors.

$$C = \varepsilon_r . C_o$$

where C_0 is the capacitance between two conductors when the space between them is vacuum, ε_r value varies from 1 for vacuum, 2.78 for Decanol oil at 0.1MHz, at 25^{o}C and 5 for normal glass. The higher the value of ε_r the higher the dielectric strength. The dielectric permittivity of material is a measure of how much the medium is polarised in the presence of an electric field compared to the free space.

1.4 Liquid dielectrophoresis

Dielectrophoresis in liquid can react differently to an electric field. In figure 2, the non-uniform electric field will make the positive charge to travel in the direction of

the negative direction. This dielectrophoresis occurs when a non-uniform electric field is applied to the Decanol, and this will create a force called dielectrophoresis force.

Dielectrophoresis forces act on materials which are either particles in the liquid or liquid in the liquid. Particle Dielectrophoresis Force (P-DEP) is the force which results from a non-uniform electric field. The particles in the fluid are subjected to both a P-DEP and also electrostatic particle-particle forces. In applications which require that the particles be manipulated individually, then the latter forces are not desirable. It is shown numerically that the ratio of the particle-particle and DEP decreases with increasing particle size and with an increasing gap between the particles (Aubry 2006). L-DEP is an electromechanical phenomenon, describing the motion of polarised liquids induced by spatially non-uniform electric fields. A neutral liquid becomes a polarised liquid only when subjected to a non-uniform electric field. The polarised liquid may be used as an actuator and conveyor and direct the liquid to the regions of high electric field intensity.

Liquid dielectrophoresis (L-DEP) is defined as the study of the effect of force which is directed on neutral dielectric liquids by a non-uniform electrical field (Pohl 1978), the liquid is assumed to be isotropic and is used to manipulate liquid substances. Liquid dielectrophoresis (L-DEP), when used at microscopic scales on top of hydrophobic surfaces, has resulted in a new way being found for rapid and automated manipulation of very small amounts of polarised liquid samples for microfluidic applications and in the development of laboratory-on-a-chip devices (Kaler 2010).

L-DEP/P-DEP made it possible to automate and rapidly classify, separate (Pethig 1996) (Hirota, Hakoda and Wakizaka 2010), and image materials ranging from

separation of DNA (Regtmeie 2010), bacteria (Arumugam 2007), chemicals L-DEP application (Reza 2010) and minerals (Ballantyne and Holtham 2010) as a P-DEP application. Liquid dielectrophoresis has been suggested for use in laboratory-on-a-chip devices as an open system for the analysis of liquids (Gunji 2000).

The dielectrophoresis principle can be explained in figure 1 and figure 2 which shows a neutral liquid and a uniform field, in which a positively charged particle will move towards the negative terminal as shown in figure 1. A neutral particle will be polarised but it will stay in the middle because it is subjected to equal forces. On the other hand a neutral liquid in a non-uniform field will be polarised and will move towards the strongest field region as shown in figure 2. The different effects on a charged particle show that the positively charged particle is moving towards the negative direction and the neutral particle moving towards the positive because of the strongest electric field.

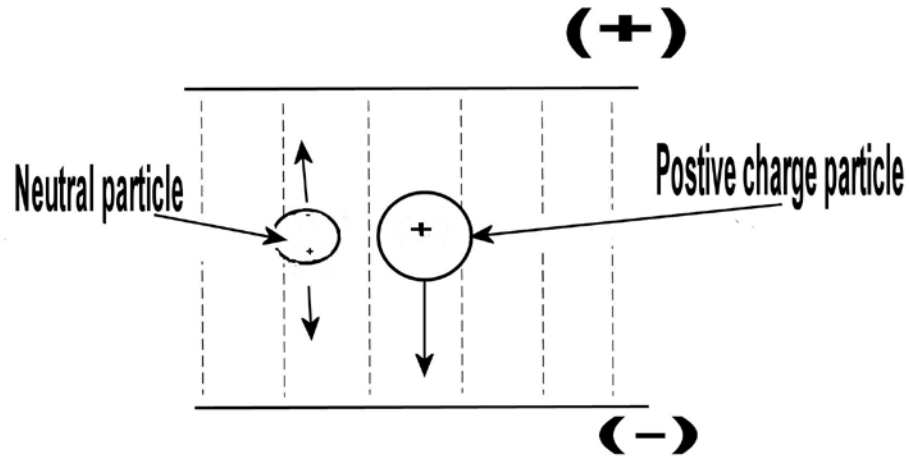

Figure 1 Uniform field on polarised particle and neutral particle

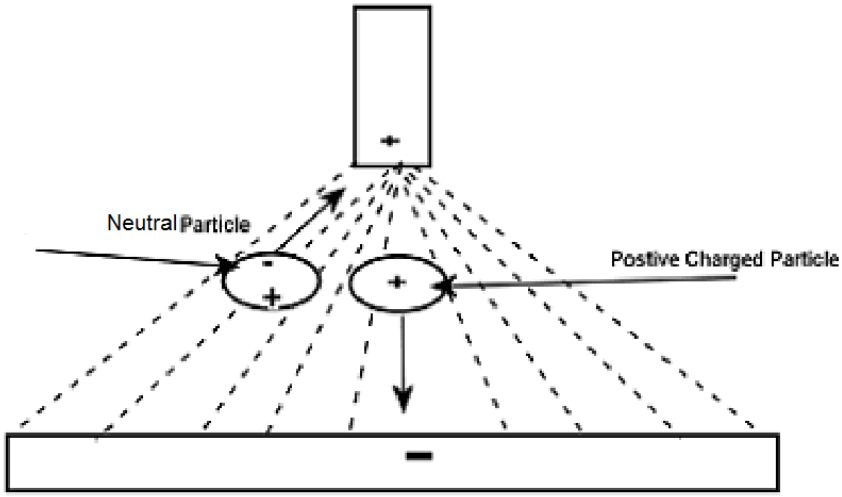

Figure 2 Non-uniform electric field

The forces which cause those movements are called Dielectrophoretic Forces (DEP) (Pohl 1978).

1.5 Dielectrophoretic Force (L-DEP) equation

As seen in section 1.4, the Dielectrophoretic Force (L-DEP) is the force which results from the interaction of a non-uniform electric field with the particles. This interaction causes the particles to be polarised. The Dielectrophoretic force (L-DEP), which is important in deciding how the dipole charge in an open system creates a force (*F*) by the non-uniform electrical field (*E*), moves as a result of applying the strongest electric field. By using Coulomb's law

$$\boldsymbol{F} = q\,.\boldsymbol{E} \qquad \text{Equation 2}$$

$\boldsymbol{F}$ is the dielectrophoresis vector force which makes the dipole moves

q is the charge

$\boldsymbol{E}$ is electrical field vector

The dipole consists of two equal charges $\pm q$ separated by a distance *l*, the distance *l* is negligible compared with the distance of other charges and *q* is large so that *q.l* is the electrical dipole moment finite *(p).*

It was noted from equation 2 that the dipole of the dielectric liquid (Barnes and Gentle 2005) will move in the electrical field under the external force (*F*).

This force will create potential energy which is the property of that dielectric liquid. There are two cases which are shown in figure 1 and figure 2, the uniform field which is shown in figure 1, the L-DEP is zero and the dipole does not move, a more complex case occurs when the dipole is in a non-uniform field (figure 2). The dipole must be considered in the *x, y and z* direction and the resultant force $\vec{F}_x$ in the x direction are given by (Lorrain and Corson 1988).

$$\vec{F}_x = \left(p_x \partial / \partial x + p_y \partial / \partial y + p_z \partial / \partial z\right)\vec{E} = \left(\vec{p}.\nabla\right)\vec{E} \qquad \text{Equation 3}$$

Where $p_x = q\mathrm{dl_x}$, $p_y = q\mathrm{dl_x}$, $p_z = q\mathrm{dl_z}$

The dipole moment p in liquid is composed of N molecular,

$$\vec{P} = N\ \vec{p}$$

P Is the dipole moment per unit volume at a given point *p*

By substituting in the *F* equation

$$\vec{F} = (N\vec{p}\ .\nabla)\vec{E} = (\vec{P}\ .\nabla)\vec{E} \qquad \text{Equation 3.1}$$

In most dielectrics P is proportional to E and is in the same direction such as dielectrics liquids which are linear and isotropic, then

$$\vec{P} = \varepsilon_0(1-\varepsilon_r)\vec{E} \qquad \text{Equation 3.2}$$

ε_r Relative dielectric constant of the dielectric medium.

This interaction induces an object force when the particle is much smaller than the electric field non-uniformities, which is given by subtitling *P* in the *F* equation 4 (Pohl 1978).

$$\nabla(A \cdot B) = (B.\nabla)A + (A.\nabla)B + B \times (\nabla \times A) + A \times (\nabla \times B)$$

Using the above vector formulas $\nabla(E.E) = (E.\nabla)E + (E.\nabla)E + E(\nabla \times E) + E \times (\nabla \times E)$

Since $\nabla \times E = 0$ from Maxwell equations and $\nabla(E.E) = 2(E.\nabla)E$

$$E = \frac{1}{2}\nabla|E|^2 \qquad \text{Equation 3.4}$$

and by substituting of equations 3.1, 3.4 in equation 3.2

$$F = \frac{1}{2}\varepsilon_0(\varepsilon_r - 1)\nabla|E|^2 \qquad \text{Equation 4}$$

F Dipole approximation to the L-DEP force, ε_0 Permittivity of free space, ε_r is relative permittivity of the medium.

Equation 4 is the L-DEP force equation and shows three important relationships. *F* has a relationship with the gradient electric field squared, *F* has a direction in the strongest resultant interface and moves irrespective of the polarity of the electrical field, and the *F* is related to the permittivity (dielectric) property of the medium.

1.6 Surface tension

Surface tension is the force per unit length acting on an imaginary line drawn on the surface between two or more different surfaces and the tendency of the surface to

keep in the minimum energy status (spherical cap in case of liquid-solid interface) (Barnes and Gentle 2005). In the case of liquid-solid interface the force inside the liquid's molecule is isotropic and the net force pulling any molecule inside the bulk liquid in any given direction is zero. The molecule of the liquid on the surface is subjected to unbalanced forces and there is a tendency of the molecule to be pulled into the bulk and the tendency of the system to minimise the area of the surface. In our open air system the drop of liquid is placed on a solid surface and triple surface tension are formed between solid, liquid and gas (air), the forces resulting from the three surface tensions will shape the drop liquid until an equilibrium position is established. The drop of liquid forms an angle with solid surface called the contact angle, water has the largest measured contact angle of 120^{o}. The contact angle of 120^{0} is used to classify the surface if it is hydrophilic (>120°) or hydrophobic (<120°).

Decanol oil surface tension is 29.8 ± 3.0 mN/m, Mercury 425.4 mN/m, water at 25^{o}C is 71.97 mN/m. Surface tension (γ) is related to liquid and surface energy (σ) is related to the solid surface and they are equal to each other.

1.7 Diffraction Gratings

Diffraction is the deviation of light from its rectilinear propagation. A diffraction grating is a set of parallel slits used to disperse light. The slits can either be apertures or obstacles. Those slits have the effect of changing the amplitude or the phase of the light wave (Hecht 2002). There are different technologies which have used diffraction gratings, the uses and applications for diffraction gratings are reported in many articles, which include fused fibres, dispersion-compensating fibre, beam

steering, Bragg gratings, optical switch (Mevel 2003), spectroscopy, communications (Senturia 2005), beam steering (Resler 1996), display (Bloom 1997) and holographic elements (Barden 1999).

1.7.1 Amplitude Diffraction Gratings (ADG)

The basic principle of ADG can be shown with reference to figure 5. The laser beam enters the square gratings pattern at a particular angle of incidence. The beam then separates into one or more "orders" according to the grating equation:

$$b \sin\theta = m\lambda \qquad \text{Equation 5}$$

where

θ = angle of diffraction

b = distance of centre to centre of the square grating (electrodes)

m = order (integers 1, 2, etc)

λ = wavelength of the incident beam

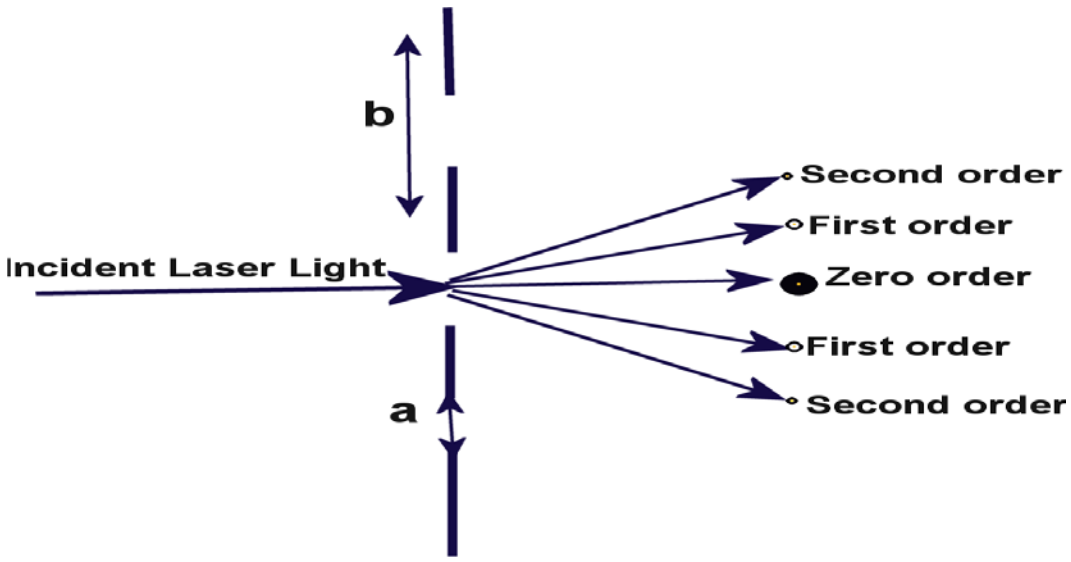

Figure 3 Amplitude Diffraction Gratings (ADG)

1.7.2 Fraunhofer analysis

Fraunhofer analysis involves an integral over the open aperture of an optical device and it relates to the superposition of amplitude in the far field which gives the intensity distribution in the far field, another analysis that is called Fresnel analysis involves the intensity distribution in the near field. Fraunhofer analysis is the analysis of the intensity of diffraction spots (see figure 3) of the parallel beam of light when the light wave approaches the diffracting slits. The diffracting slit is very small compared to the distance of the image source. Fraunhofer analysed various types of diffracting objects which include one slit, double slit, and multiple slits. For multiple slits, the Fraunhofer Intensity is

$$I(\theta) = \frac{I(0)}{N^2}\left(\frac{\sin\beta}{\beta}\right)^2\left(\frac{\sin N\alpha}{\alpha}\right)^2 \qquad \text{Equation 6}$$

$\alpha = \frac{ka}{2}\sin\theta$, $\beta = \frac{kb}{2}\sin\theta$, $k = \frac{2\pi}{\lambda}$, $I(0)$ is the incident laser beam, N number of gratings patterns.

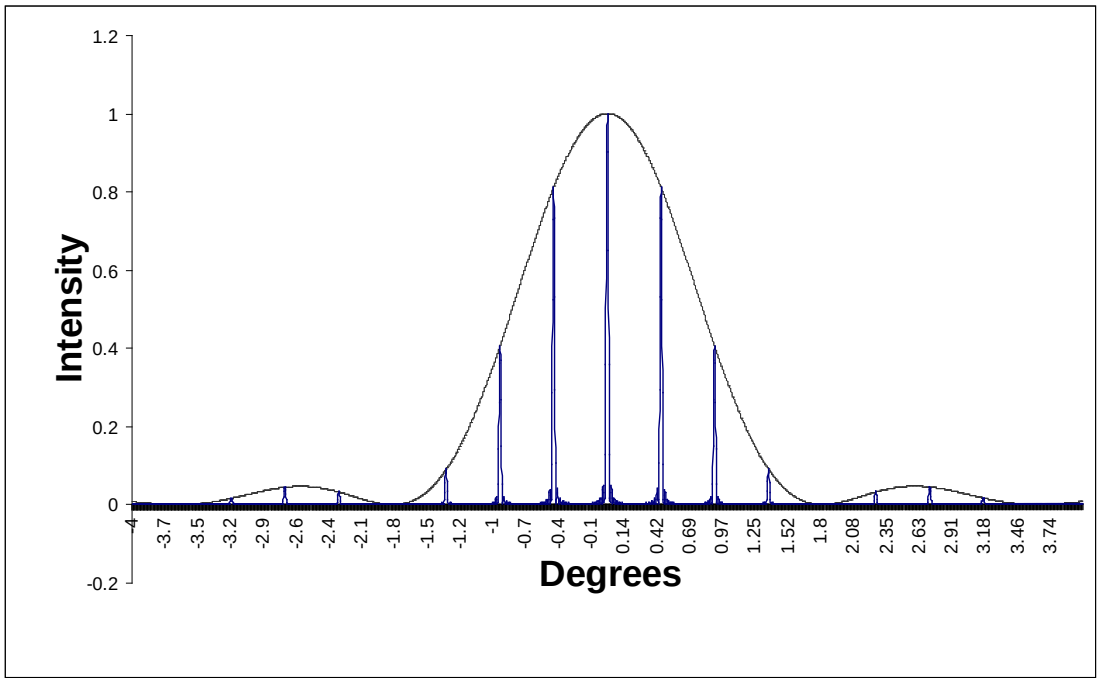

Figure 4 Multi amplitude diffraction grating relationship for a=4b, N=20

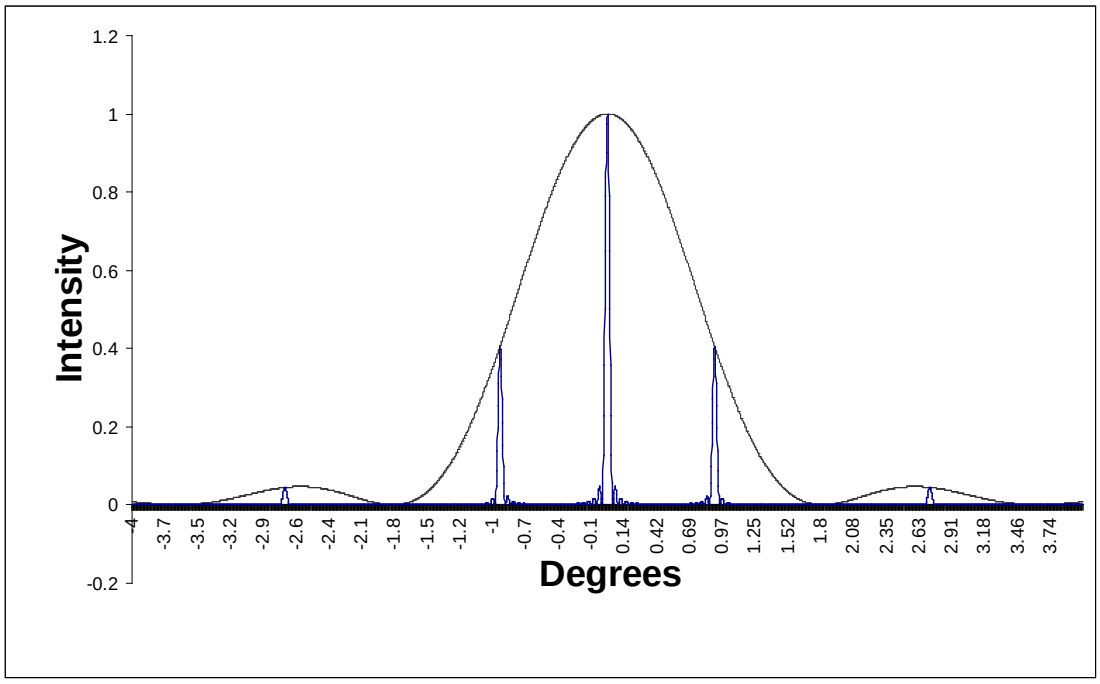

Figure 5 Multi amplitude diffraction grating relationship for *a=2b, N=20*

Equation 6 is the general equation which shows the relationship between the parameters of the ADG. Figure 4 shows the relationship for a specific case when

b = 4a and shows the effects of changing the electrode gap, where *N*, the number of gratings (slits) is equal to 20. The maximum diffraction pattern for N = 20 and b = 20a that occurs at 0, 0.97, -0.97, 2.63, -2.63, as shown in figure 5. From equation 6 it can also be shown that by changing the ratio of (*a/b*), the diffraction spots can be moved to the position of the first order and so on.

1.7.3 Phase Diffraction Gratings (PDG)

In the amplitude diffraction grating a slit with different ratios (*a/b*) is used. Most optical materials are isotropic and have one refractive index. In the Phase Diffraction Gratings (PDG), two or more materials can be used to vary the refractive index and diffract the laser beam. The Optical Path Length (OPL) is the indicator parameter of the phase difference in the laser light wavelength after the light passes through material with a different refractive index; the thickness of the material makes the refractive index change its Optical Path Length (OPL) and creates a diffraction pattern. A zero OPL means the material has the same phase and one refractive index. In simple terms to calculate OPL is to multiply the physical distance times the refractive index. This principle is used in the optical device in chapter 2.

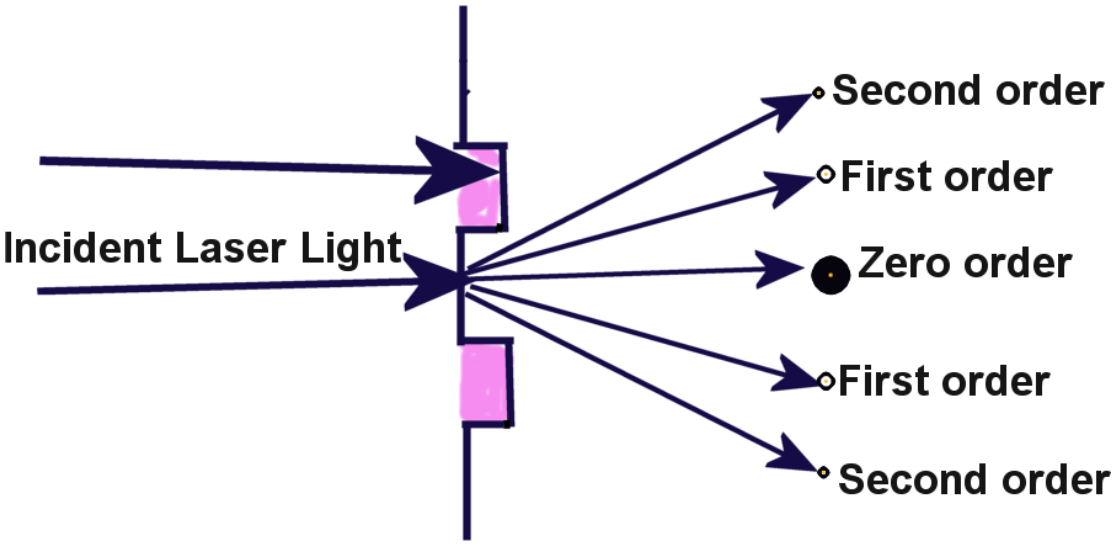

Figure 6 Phase diffraction gratings

1.8 Thick gratings

A thick phase gratings that operates in a cell contains liquid or transparent crystal and is one of two physical regimes that is also called the Bragg regime (Hecht 2002). The other regime is thin gratings which are shown in section 1.9.

The Bragg regime is considered in many reports as a term referring to gratings which follow Bragg diffraction (Aubry 2006). Bragg diffraction occurs when the laser wavelength is comparable to the atomic spacing. The atoms in Bragg diffraction scatter the laser light and the constructive interference follows Bragg law and a diffraction pattern cannot happen. Equation 7 shows the Bragg law, and it states that a beam of parallel waves incident at an angle θ reflects at an angle θ from the plane. In dense layers of atoms with spacing d, when the path difference consists of a whole number of wavelengths, the reflected waves interfere constructively.

$$2d \sin\theta = n\lambda_0$$ Equation 7

Where d is the spacing between the atomic spacing

n is integer

λ is the laser wavelength

θ is the scattering angle

1.9 Thin Gratings

A thin grating is the other type of physical regime for phase gratings, and is defined as gratings which follow a Raman-Nath regime (Hecht 2002). Raman showed that thin gratings produce a Bessel function relationship between the wavelength amplitude and the light intensity in a diffraction order. Nath followed the steps of Raman and proved that Raman was correct. Nath gave the relative intensity of the mth diffraction order to the nth diffraction order as in equation 7.1 which shows the relationship between different diffraction orders as a condition for thin gratings.

$$\frac{J_m^2\left[\frac{2\pi mh}{\lambda_0}\right]}{J_n^2\left[\frac{2\pi mh}{\lambda_0}\right]}$$ Equation 7.1

n Maximum variation of the refractive index

h The optical path length

J_m^2 Bessel function at m diffraction order

J_n^2 Bessel function at n diffraction order

Acousto-optic cells are an example of a technology which can operate in the above two regime systems, depending on the sinusoidal drive voltage of frequency f_c and the acoustic velocity V characteristic of the medium. This interaction between the acoustic velocity and the f_c will induce a phase grating with period (V/f_c), which will interact with the laser beam and produce a diffraction pattern as explained in Fraunhofer diffraction section 1.7.2. In the Raman-Nath regime, the laser beam is phase modulated by the moving refractive index grating which produces a complex transmission function of the amplitude of the transmitted signal as in equation 8 (Goodman 2005)

$$U(y:t) = U_0 \exp\left\{ j\frac{2\pi\sigma d}{\lambda_0} A\left(\frac{y}{V} + t + \tau_0\right) \times \sin\left[2\pi f_c\left(\frac{y}{V} + t - \tau_0\right) - \psi\left(\frac{y}{V} + t - \tau_0\right)\right]\right\} rect\frac{y}{L} \quad \text{Equation 8}$$

V is the acoustic velocity propagation of the liquid

Y is distance travelled

t is instant of time σ is the proportionality constant τ_0 Time delay through the optical path length *L* is the length of the wave propagation, *rect* is the rectangular function *U* is the transmission function of the amplitude of the transmitted signal.

Raman-Nath regime definition is simplified by (MOHARAM 1980) and that it is defined with respect to the diffraction efficiency η of the grating

$$\eta = J^2\left(\frac{2\pi n_1 d}{\lambda \cos\theta}\right)$$

where n_1 the amplitude of the sinusoidal refractive index grating, *d* is the thickness of the grating, λ is the free-space wavelength, and θ is the angle of incidence inside the grating. η is the fraction of the incident optical intensity in a single diffraction order. Moharam (MOHARAM 1980) concluded for each criterion is different for

different set of applications, however it is clear that the existence of the diffraction orders (0, 1, 2,..) is enough to classify the application under Raman-Nath regime.

1.10 Thin sinusoidal phase grating

The variation of a thin layer of material and the change to its shape, to form a sinusoidal wave shape is defined as thin sinusoidal phase gratings. A device can be used as switchable phase grating by utilising a ferroelectric liquid crystal (FLC) mixed with a photo curable liquid crystal using a simple one-step process (Matsumoto 2006).

1.11 Voltage programmable diffraction grating device

The voltage programmable diffraction grating device first idea was patented as a fluidic switchable phase grating by varying the phase and direction of light passing through the gratings inside an enclosure of two fluids (Brown, Newton and McHale 2006). The idea was refined to single fluid which is made to form a thin sinusoidal gratings using L-DEP. The purpose of a thin sinusoidal phase grating is to deflect energy out of the zero order into the other higher diffraction orders under Raman-Nath regime. Figure 7 shows a layer of liquid before and after applying a non uniform electric field.

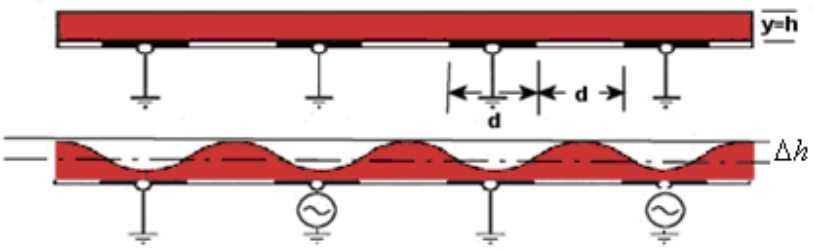

Figure 7 Sinusoidal phase grating

The Modelling relationship for the thin sinusoidal phase grating was derived (Brown 2009) and it was shown in Appendix A to be

$$\Delta h = \left[\frac{16\varepsilon_0}{3\gamma\pi^4}\left(\varepsilon_{oil} - \varepsilon_{air}\right)\exp\left(-\frac{4\pi h}{d}\right)\right]V^2 \qquad \text{Equation 9}$$

Δh is the varation of the oil thickness amplitide under non-uniform electric field

$\boldsymbol{V_0}$ is the applied 20khz ac voltage

ε is the dielectric constant of air and oil

γ is the surface tension

d is the electrodes width

h is the oil thickness

p is the pitch and it is equal to 2d (Figure 7)

Equation 9 shows the relationship between the peak-to-peak amplitude of the wrinkle Δh which is affected by the average thickness *h* of the oil film and the pitch *p* of the wrinkle, the non-uniform field, the liquid mechanical properties and the surface tension of the liquid.

1.11.1 Fraunhofer analysis of thin sinusoidal phase grating

Fraunhofer analysis of a thin sinusoidal phase grating drives the intensity's mathematical manipulations. This mathematical calculation is done for field wave propagation. The analysis deals with various input field distributions similar to equation 8 and derives the intensity equation (*I*) using Fourier for a thin sinusoidal grating (Goodman 2005). (*I*) is the intensity equation of sinusoidal phase grating.

$$I(x,y) \approx \left(\frac{A}{\lambda z}\right)^2 \sum_{q=-\infty}^{\infty} J_q^2\left(\frac{m}{2}\right) \sin c^2\left[\frac{2w}{\lambda z}\left(x - qf_0\lambda z\right)\right] \sin c^2\left(\frac{2wy}{\lambda z}\right) \qquad \text{Equation 10}$$

From equation 10, it is shown that the intensity equation is proportional to the Bessel function $J_q^2\ \frac{m}{2}$

where *m* is the optical path length relative to the amplitude of the sinusoidal thin layer in equation 10 and *q* is the diffraction order.

1.11.2 Fraunhofer analysis Bessel functions

The Bessel function in equation 10 is used to compare the experimental surface profile graph with normal transmitting and focusing of laser beam through an optical system. Figure 8 shows a typical Sinusoidal Phase Grating Diffraction efficiency which shows the plot of η_q vs. *m/2* in the Bessel term in equation 10 and figure 8 is used as a measure of how the experimental results compares to the Fourier transform response of thin sinusoidal phase grating optical system.

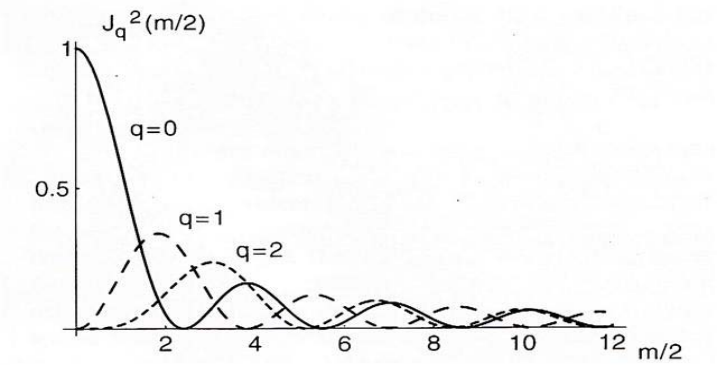

Figure 8 Sinusoidal Phase Grating Diffraction efficiency (Hecht 1987)

1.12 Interferometry

There are several methods to measure the thickness of a thin layer of liquid, such as Optical Coherence tomography (OCT), Stylus profilometry, laser triangulation, confocal microscopy, digital holography, AFM and interferometry.

Optical coherence tomography (OCT) is used in biomedical imaging (Lee 2009), opticians, and other art applications which require micrometer accuracy and also up to a millimetre depth resolution. The stylus profilometry is a contact method which requires a reference and it is not suitable for measuring a wrinkle on a liquid surface. The other methods which are mentioned above, such as laser triangulation (Welch 2010), digital holography (Song 2010), and AFM, are methods which are used for measuring the thickness of very tiny objects and require time to obtain the results and are also expensive.

Interferometry is the least expensive method and it can be deployed easily to the experimental set up to measure the thickness of liquid in different locations on the

thin film of liquid while the voltage is applied. Mach-Zehnder Interferometer is the choice as a tool to observe the thickness and wrinkle. Mach-Zehnder interferometer is already used to characterise a small-size gratings (Lee 2003)

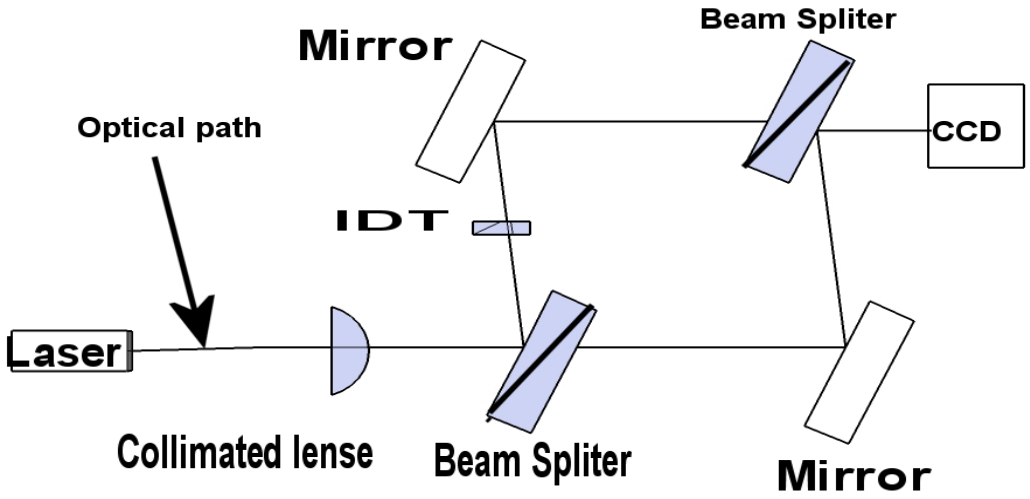

Figure 9 Mach-Zehnder Interferometer

The principle of Mach-Zehnder interferometer is shown in Figure 9. The Mach-Zehnder interferometer operation is based on creating a phase shift when the device is placed in one of the two arms.

The interferometer is an important tool in characterising the device by verifying the relationship between the phase shift which is created as a result of voltage applied to the device and the height of the liquid gratings. It is also used to measure the thickness of the thin layer of liquid in the device, and the phase shift in the interferometer can establish the switching relationship of the on-off of the gratings in the dynamic analysis.

The interferometer uses a 17mW laser, a spatial filter system to produce a Gaussian profile on an expanded beam, an half wavelength Rhomb-Fresnel filter, a polariser,

several tilting mirrors, two beam splitters, a set of various focal length lenses (Shaoulov 2002).

A relay lense system, two microscope objective lenses and a CCD camera (Lee 2003), chapter 2 will explain the method in more detail and chapter 3 will the show the images.

Chapter 2: Methods and materials

2.1 Introduction

Chapter 2 will describe the main components of the Variable Phase Grating Optical Device (VPGOD). This research is a continuation of the previous research which established various principles of Variable Phase Liquid Optical Device (Brown 2009) based on dielectrophoresis. This research is focused on a novel optical device operating on the principle of dielectrophoresis only. The purpose of the device is to divert the energy of light waves into separate diffraction spots by creating a wrinkle on the surface of the liquid. The previous research used Hexadecane oil and provided preliminary results suggesting a possible use of Decanol oil. It was shown that Decanol oil can be used to provide a sinusoidal wrinkle at lower voltages than Hexadecane, but did not provide a systematic experimental study which verifies the mathematical physical relationship. This research will characterise the Optical Device with Decanol oil and look at the static and dynamic experiments of the wrinkle on the surface of a thin micro layer of liquid to redirect a coherent light (laser). The previous work (Wells 2009) looked at various thin micro layers of liquid in optical devices and started characterising voltage programmable liquid optical devices and Hexadecane was chosen to be studied for static set of experiments. This research will look at the systematic approach for another liquid (1-Decanol) and start exploring the dynamic characteristic of the liquid. The experimental results will be related to the mathematical model equation 9 in chapter 1.

2.1 Device Construction

The main components of the device are shown in figure 10. The components of the device are: Interdigitated Transducer (IDT), with electrodes etched on an Indium Tin Oxide (ITO) coated glass, a thin layer of SU8 and a thin layer of Decanol. The schematic diagram of figure 10 is shown with a side view of the optical device under a non uniform electric field (L-DEP forces) as shown in chapter 1. V_0 is the voltage which is supplied to the IDT to generate the L-DEP force when a thin layer of Decanol is put on the surface of the IDT as in figure 10.

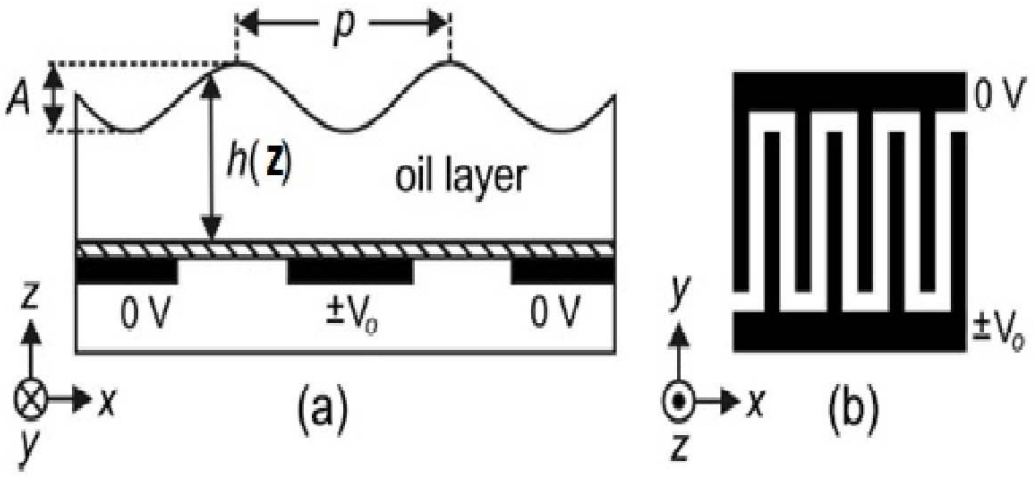

Figure 10 Schematic diagram of the device (Brown 2009)

2.2 Device fabrication

The IDT of the device, as shown in figure 10, is used with Decanol oil to modulate the phase of light. The IDT and Decanol oil are the vital parts in all the experiments in this research. The electrodes are made of ITO (Indium Tin Oxide) etched on glass and the ITO electrodes are connected to an AC power supply to provide the L-DEP

forces. The combination of ITO, Decanol oil and the L-DEP forces provide an important role in the experiments as it provides a non-uniform electric field to cause the surface of the thin layer of Decanol oil to deform. The surface deformation (undulation) causes the surface of the thin layer of Decanol oil to act as a variable phase diffraction grating.

The phase diffraction gratings can be of several types, but the main type, which is used with the optical device electrodes, is the continuous changing of the optical path length of the laser light which passes through oil/air. The optical device has a refractive index mismatch, as shown figure 6 in chapter 1. The change of the Decanol oil undulation height depends on the type of oil used, applied voltage difference between the electrodes and the spacing between the electrodes. The variation in height of the Decanol oil relates to the variation in intensity of the diffraction spots. The electrodes have another function, besides providing a non-uniform electric field for a thin layer of Decanol oil surface, and that is to provide the undesired amplitude diffraction gratings (ADG).

2.3 Photolithography method of making IDT electrodes using s1813 photo resist

The current main approach for making the IDT for the device is to use micro-photolithography in a clean room environment in order to fabricate the IDT for different sizes of electrodes.

The process is to spin the ITO coated glass with s1813 photo resist in order to cover it with a thin layer. The s1813 photo resist method is more preferred method for high

voltage applications that is required to produce the required DEP force in the dielectric material and it was chosen for this research to make the Interdigitated Transducer (IDT).

The Interdigitated Transducer (IDT) was made at different pitch sizes from 10 μm pitch (5 μm electrodes gap) and up to 320 μm pitch (160 μm electrodes gap) for the use in the static and dynamic experiments. The photolithography method involves cutting the required size of glass coated ITO, cleaning the samples, spin coating with s1813, baking, exposing s1813 photo resist to UV light with a mask which has the same gap-space distance with a rectangular shape and different sizes of electrodes. A developer solution is used to develop the electrodes, etching the excess ITO and rinsing with acetone, and finally to dry the electrodes.

The following steps are used to manufacture the electrodes of the IDT optical device:

- Decon 90 with deionised Water at 5% Decon 90 concentration in a beaker for cleaning the sample. The purpose of this step is to clean the sample from any dust or small particles which might cover the ITO and causes the sample to have short circuits between the electrodes.
- Using the Ultrasonic bath (make: GUSON). The purpose of this step is to remove grease (e.g. finger prints) and other dust still sticking to the surface for 10 minutes. The IDT devices are cleaned with de-ionised water only plus Isopropanol (IPA) and the devices are dried with nitrogen.
- Spin coating (Laurell model WS-6505-6NPP/A2/AR2) is used with s1813 positive photo resist. The purpose of this step is to provide another layer to cover the ITO with s1813 photo resist.

- A precision hot plate is used in the pre baking at 95^0C for 75 seconds. The purpose of this step is to make the s1813 ready for the mask aligner step and the time of 75 seconds was used as an optimum value for a successful IDT. This stage will increase resist sensitivity, thus requiring shorter exposure times
- The mask is designed for electrodes between 5μm - 200μm, as shown in figure 10b. The purpose of the mask is to cover the s1813 photo resist from the ultra violet light.
- The purpose of this step is to expose the s1813 photo resist areas, which are not covered by the mask, to ultra violet light. The mask aligner which is used is of type (SUSS MicroTech Lithography GmbH MJB4).
- S1813 developer was used to develop the electrodes of the IDT. The purpose of this step is to remove s1813 which was not covered by the mask and was not exposed to UV light.

- In this step the IDT electrodes are post baked at 115^0C for 15 minutes. The purpose of this step is to help in strengthen the electrodes in the samples.
- In this step there are two types of acid which have been used to etch the optical device; Oxalic acid or Nitric acid depending on the ITO layer has been deposited on the glass slide. In the dynamic optical device of size 10, 20, and 40μm, Oxalic acid was used for 10 minutes. This time was reasonable to remove all the ITO which was developed with the s1813 developer.

In the static analysis, a new patch of ITO was used and the oxalic acid required long time to complete the etching of ITO. It was decided to use a stronger acid, namely nitric acid (HNO_2). The reason for this variation in this step depends on the method

of depositing the ITO on the glass slide. This step was for optical devices of sizes 80μm, 120μm, and 160μm electrodes gaps. The HNO_2 completed the etching in a few minutes. The HNO_2 was concentrated at a ratio of 1:12.5 water:12.5 HCl_2. The time to etch was approximately 6 minutes. The use of HNO_2 speeds up the etching process.

- The s1813 photo resist which is still covering the ITO of the optical device is removed with acetone acid. The optical device is washed with ionised water and dried.

2.4 The IDT's Coatings

There are three choices for the IDT's coating, SU8, SiO_2, or no surface coatings.

2.4.1 SU8 processes

SU8 photoresist is a thin polymer layer which is used to protect the electrodes of the optical devices from the high voltage and to make the surface less hydrophobic. SU8-2 is used to cover the electrodes and the SU8 thin layer is approximately 2μm thick. The layer can be made thinner than 2 μm by mixing SU8-2 with SU8 developer at various percentages. A layer of 0.5μm was used for the static experiments and was achieved by mixing 50% SU8-2 with a 50% SU8-2 developer. The second purpose of the SU8 is to help the thin layer of Decanol oil to spread and make the IDT less hydrophobic. The process can be summarised as

- washing the finished IDT devices as explained in section 2.2

- S8-2 is spun on the IDT at 500 rpm for 5 seconds and then 3000 rpm for 30 seconds as described in section 2.2
- the IDT device is pre baked for 1 minute at 65^0C and the temperature is increased to 95^0C in steps of 20^0C/minute for 2 minutes
- the IDT device is then exposed to Ultra Violet (UV) light for 6 seconds to support the polymerisation in the same mask aligner without a mask to harden the SU8 polymer.
- the final step is to post-bake the IDT device for 2 minutes at 65^0C and again increase the temperature to 95^0C in steps of 20^0C/ minute for 5 minutes and a finally bake at 175^0C for 30 minutes to make the surface hard.

The thicker the layer of SU8 the smoother is the surface but will add to the phase shift in the path of the laser beam. This process is very important to understand the way the diffraction process with the minimum thickness of SU8.

2.4.2 SiO_2 coatings

The IDT was coated with a layer of thickness between 0.5 to15μm thickness of SU8 and the thicker the layer of SU8 will result in more phase shift that will add to the path of the laser light. As the result of this extra phase shift it was attempted to use the IDT without a zero layer of SU8 coating, however it was noted that the Decanol oil does not spread correctly on the surface of the IDT and the surface becomes more hydrophobic. As an alternative material to SU8 coating, SiO_2 was attempted to coat the IDT using the sputtering method. SiO_2 is an inorganic material which has many advantages to the organic SU8.

- SiO_2 coats the surface of the IDT well with a very thin layer from 25 nm
- It is process which does not require clean room conditions
- It has a high resistivity and dielectric constant

It was noted that SiO_2 makes the surface of the IDT hydrophobic, which means higher voltages are required to spread the Decanol oil. It was also noted that SiO_2 has a high contact angle of 36^0 compared to SU8 of 5^0. It is clear that SiO_2 requires extra force to make it hydrophobic like SU8. The contact angle was measured as seen in figure 11, which shows the 1-Decanol oil on the SiO_2 surface. Table 1 shows the SiO_2 material properties.

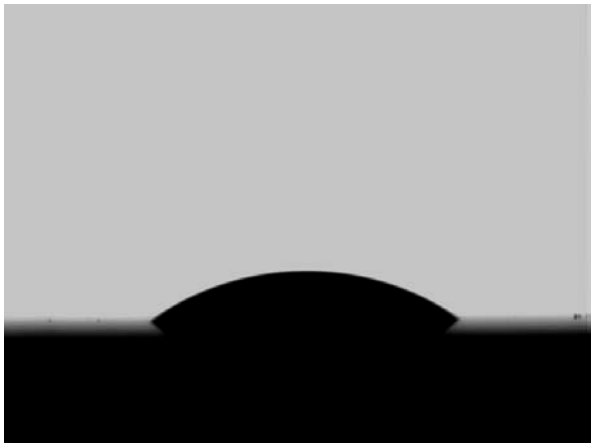

Figure 11 Decanol SiO_2 contact angle

Table 1 SiO_2 material properties

Material	***Quartz***	***Fused silica***
Density (g/cm^3)	2.65	2.2
Thermal conductivity (Wm^{-1} K)	1.3	1.4
Thermal expansion coeff. (10^{-6} K^{-1})	12.3	0.4
Tensile strength (MPa)	55	110

Dielectric field strength (kV/mm)	15.0-25.0	15.0-40.0
Resistivity (Ωm)	10^{12}-10^{16}	$>10^{18}$

2.5 Static and dynamic experimental setup

The objectives of the static and dynamic experimental set up are to observe and to prove that the ac voltage applied (V^2) has a relationship with the wrinkle amplitude and this relationship follows a mathematical model derived in appendix A. In the dynamic experiments other relationships are observed mainly the Bessel function and the switching time. In both experiments the thickness of the oil is observed and measured.

This is achieved by applying a non-uniform electric field (AC voltage at 20 kHz) to the optical device; this non-uniform electric field will create a Dielectrophoretic force (L-DEP) in the Decanol which makes the liquid undulate. The voltage applied is the ac voltage which makes the Decanol oil creates a ripple effect, as the result of Dielectrophoretic force. This L-DEP force makes the Decanol polarise in the direction of the strong electrical field. Two sets of experiments were set up to examine the V^2 relationship with different parameters in the optical device, Decanol thickness, amplitude of wrinkles, electrodes gap, thickness of SU8 layer which is used in the optical device are observed to test the mathematical approximation of the model to the experimental results.

2.5.1 Static experiments layout

The Mach-Zehnder interferometer, as described in Chapter 1 is used to measure the wrinkle amplitude. The Mach-Zehnder interferometer operates by splitting the He-Ne laser into two separate beams. Along the beam of laser light there are two reflecting mirrors and two focusing lenses to relay the image to the CCD camera. Adjustment and setting of those lenses and mirrors is important to focus the image of the fringes. The static experiment is shown in Figure 12. The ac voltage power supply was used to provide the non-uniform electric field.

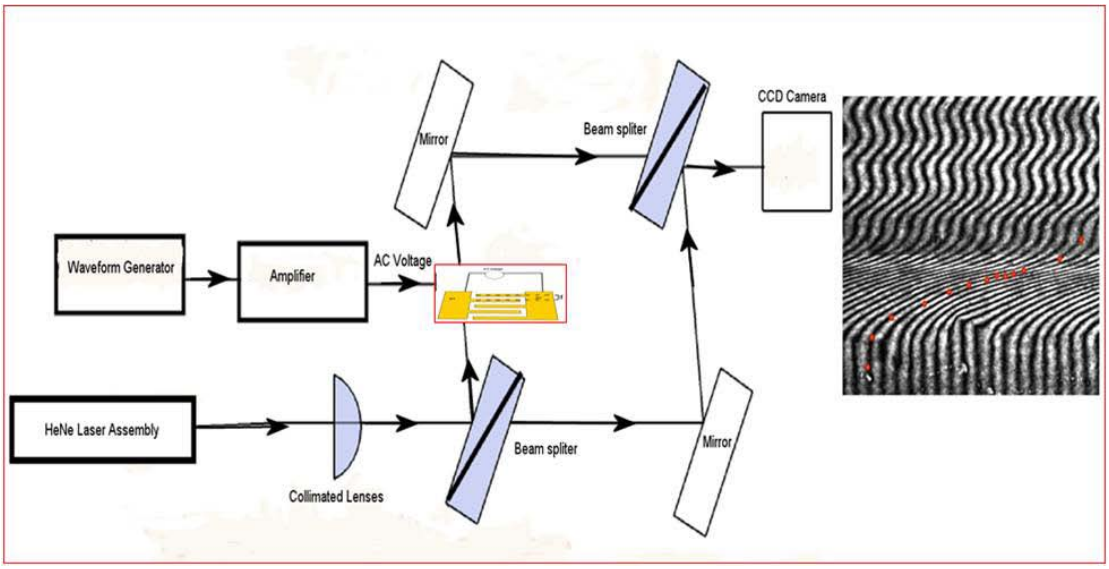

Figure 12 Static experiment set up

The static experiment uses TGA1241 Arbitrary waveform Generator, Trek Model PZD700 M/S amplifier system and Agilent 34401A meter, Thorlabs CCD camera, and Mach-Zehnder interferometer, sample holder and Dell lap top PC to view and save the images of the interferometer. The experiments use electrodes with gaps of 80μm, 120μm and 160μm Interdigitated Transducers (IDT) to characterise the above mentioned relationships.

The static analysis mainly uses the amplified sinusoidal waveform generated by the waveform generator at 20kHz and amplified by the Trek amplifier system to produce high voltages at that frequency, which act like an AC power supply with a 20 kHz variable ac voltage. 20 kHz was chosen because the system responds well to that frequency. The thin sinusoidal phase diffraction gives the best reaction for a frequency below 50 kHz. As a result of applying a sinusoidal ac voltage with 20 kHz to the surface of the Decanol oil, the thin layer of Decanol oil starts to wrinkle. This wrinkle height in the Decanol oil surface is observed using Mach-Zehnder interferometer at several different voltages. Chapter 3 shows the results of the Static analysis.

2.6 Static experiment procedure

The Mach Zehnder interferometer is used to image the Decanol surface under a non-uniform electric field. The following method was used to analysis those images and convert those images into oil thickness and amplitude of the wrinkle undulation in meters..

2.6.1 Measuring the amplitude in pixels

The pixel shift in the wrinkles undulation is converted into surface height by importing the interferometer's images of oil surface wrinkle into Image-J software and local four troughs and peaks in pixels, as shown in see figure 13. Four troughs and peaks were chosen for accuracy and to check that oil is spread properly and the amplitude is the same across four undulations. The difference of the length between

the troughs and peaks are averaged and equation 14 is used as in section 2.7 to convert pixel shift to surface height.

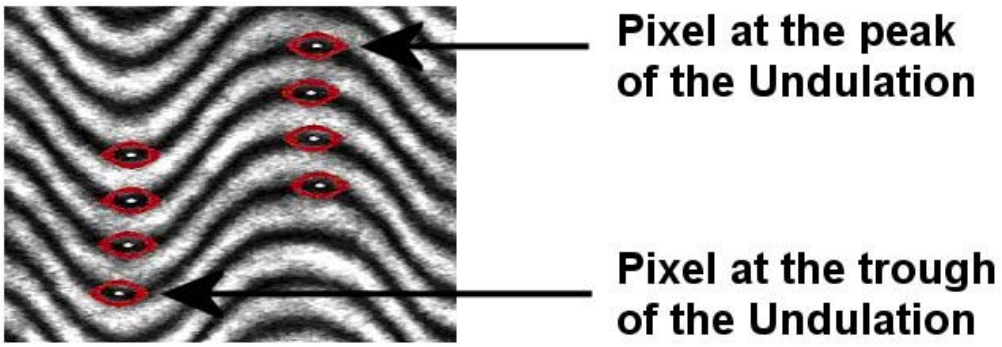

Figure 13 Positions of the pixels used for measurements of the amplitude

2.6.2 Measuring the layer thickness in pixels

The interferometer image of the edge of the Decanol oil surface is analysed by using image analysis software. The edge of the Decanol oil surface represents the thickness of the spread Decanol oil drop. The raw image is exported to the software package and the changes to fringes are marked as shown in figure 14. Six fringes are marked such that the average fringe shift is measured, as marked in figure 14 as column 2 and column 3.

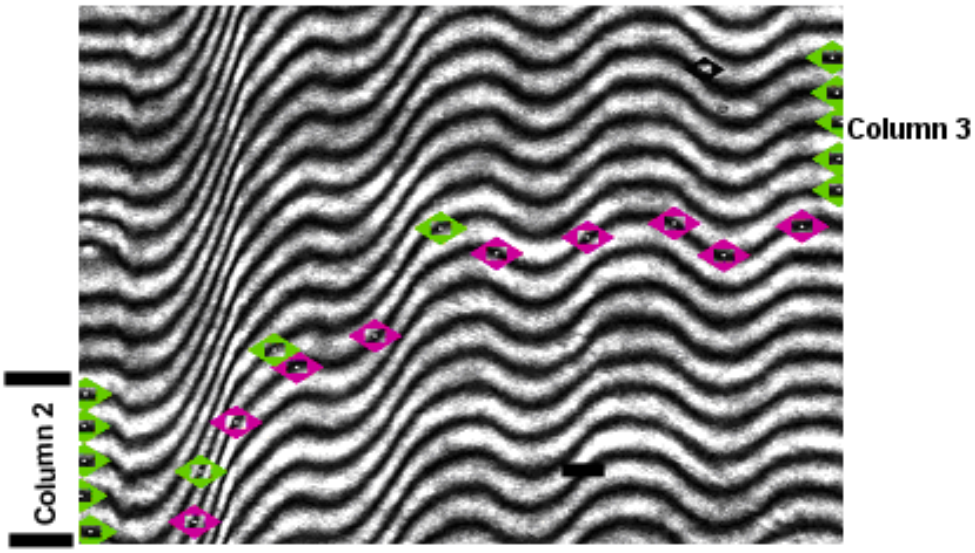

Figure 14 Edge image for oil thickness measurement

The position of the fringe in pixel in the region outside the electrodes is recorded as shown in figure 14 column 2. The same process is carried out for the next six consecutive fringes.

The positions of the same fringes are recorded inside the thin layer of 1-Decanol oil column 3 as show in figure 14. The difference between the two values is then calculated to give the relative fringe shift in pixels.

In order to calculate the number of fringes shifted, the average number of pixels must be calculated between the fringes. This is done by plotting the pixel position against the fringe number for six fringes on the same image. Figure 15 shows an example plot of this data and the regression fit gives the average pixel spacing. The average relative fringe shift in pixels (f_p) is divided by the average pixel spacing (A_p) to give the number of fringes shifted (N_f). See equation 11

$$\frac{f_p}{A_p} = N_f \qquad \text{Equation 11}$$

A_p is the slope of the straight line equation of Figure 15.

Figure 15 Pixel to length Conversion factor

The number of fringe shift (N_f) is converted to thickness in metres by substituting the value of N_f in equation 11 and using the Decanol oil refractive index with the air refractive index.

The parameters of refractive indices of Decanol oil and air and wavelength of laser light are substituted into equation 14 and used to calculate the oil thickness or wrinkle's amplitude in meters.

2.7 Converting fringe shift into surface height change

The surface height in fringe shift is converted into height in μm, by considering the change in the optical laser light path vector travelling through different regions. Figure 16 shows the different regions and the thickness which the laser wave travels.

$\Delta h = h2 - h1$

k is the wave vector

k.r is the wave vector and the distance travelled

$$k^{\rightarrow}.r^{\rightarrow} = \frac{2\pi}{\lambda_0}\left(\left(h_1 + \Delta h\right)\cdot n_{oil}\right) \qquad \text{Equation 12}$$

If one complete fringe movement is set equal to 2π then the difference in optical path length is

$$\frac{2\pi}{\lambda_0}\left(\left(h_1 + \Delta h\right)\cdot n_{oil}\right) - \left(h_1 \cdot n_{oil}\right) + \Delta h \cdot n_{air})) = 2\pi \qquad \text{Equation 13}$$

By rearranging equation 13, in terms of the changes in height inside the optical device, the fringe shift can be measured as is shown in figure 16 below.

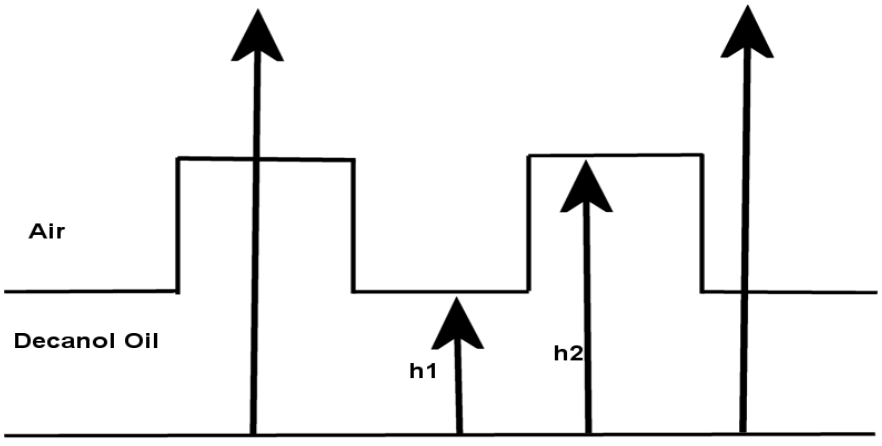

Figure 16 The thickness measurement assumptions

$$\Delta h = N_f \times \frac{\lambda_0}{n_{oil} - n_{air}}$$ Equation 14

Δh is the difference of the length of the optical path in the Decanol oil (h1) and air (h2)

N_f Number of fringe changes

n_{oil} Refractive index of Decanol oil=1.435

n_{air} Refractive index of air ≈ 1

λ_0 Wavelength of Laser light

$$\Delta h = 2.3 \times (N_f) \times \lambda_0$$ Equation 15

The ac voltage at 20 kHz is increased from 88V r.m.s to 292V r.m.s. The amplitude is measured at peak and measured at trough as shown in the chapter 3. The results for amplitude variation under various thicknesses of Decanol oil are plotted against V^2 as shown in chapter 3. Those steps were repeated for 8 oil thicknesses for each IDT of electrodes gap 120μm, 80μm and 160μm.

The final step is examining the modelling relationship in equation 9.

$$\Delta h = \left[\frac{16\varepsilon_0}{3\gamma\pi^4} (\varepsilon_{oil} - \varepsilon_{air}) \exp\left(-\frac{4\pi h}{d} \right) \right] V^2$$ Equation 16

All the results of those steps are shown in chapter 3, for electrodes gas120μm, 160μm and 80μm.

2.8 Dynamic analysis

The aim of the dynamic analysis is to study to estimate the switching response time of the wrinkle that is to apply the physics which was shown in Chapter 1 section 1.10. The previous research touched on this subject and reported the possibility of achieving a fast switch on, and physically it represents a Bessel function. In this analysis, a second experiment which is called the dynamic analysis of the optical device was set up in order to establish a systemic study for the use of the optical device with Decanol oil as a fast optical switch. The dynamic experiment uses an oscilloscope, signal generator, amplifier, and meter, power supply for CCD camera, Mach-Zehnder interferometer, sample holder and lap top to view and save the images of the interferometer and uses IDT of electrodes gap 20μm and 40μm only to provide the L-DEP and determine the switching time of the wrinkle. The main purpose of the dynamic analysis is to observe the optical device as a switch on and off as a function voltage, electrodes gap and liquid film thickness. A thin layer of Decanol oil is applied to the centre of 20μm and 40μm (electrode width and gaps). In this experiment two types of optical devices were used, one was with no layer of SU8 and the second type of optical devices are optical devices which were coated with 2μm of SU8, and 15μm layer of SU8. The variable signal generator was set up to 20 kHz square wave with Amplitude Modulation (AM) of the triangular wave 1-20 Hz. The switching effect is as a result of creating a fast undulation in the surface which can be detected by the photo detector DT 36A. The relationship between the amplitude variation of Decanol and applied voltages was recorded. The switching time vs. the thickness of Decanol was observed.

2.8.1 Dynamic Analysis Procedure

An experimental procedure was used for characterising the dynamics of Decanol undulation under the electric field of various IDT samples (40μm, 20μm, 10μm, 5μm). Two IDT samples were used (40μm, 20μm). The procedure is to check the intensity of the zero order, first order and second order variations with the voltage applied. The experiment was set to the maximum and minimum voltages of triangular waveform without the IDT sample. The triangular waveform setting represents the minimum voltage that starts the wrinkle and the maximum voltage for the peak of the wrinkle. The oscilloscope was checked for the waveform and the amplifier was "trimmed" to give the best 20 kHz square wave shape at the IDT sample. The triangular amplitude modulated waveform was used for spreading the oil and for investigating the quasi-static voltage dependence of the diffracted spot intensities. The squarewave leading and trailing edges were used to investigate the speed at which different diffracted spots change intensity when the amplitude of the voltage is suddenly increased (leading edge) or suddenly decreased (trailing edge). The next stage is to apply 1-Decanol oil and check that the oil spread with the triangular wave amplitude modulated 20 kHz waveform.

A snapshot of the interferometer fringes at the edge of the spread oil is taken for oil thickness measurement with the triangular amplitude modulation switched on (when it is near the low voltage) and with the triangular amplitude modulation switched off. The angle, voltage waveform of photodiode detector on zero order spot, first order and second order are recorded.

The triangular waveform is changed to 20 kHz square waveform with 0.2 Hz amplitude modulation and the voltage waveform were recorded before and after the photodetector. For square wave, leading and trailing edges were recorded for switching time response for zero order, first order and second order to measure the switching time response. At each diffraction order, the thickness and angle are recorded by taking thickness measurement.

The procedure is repeated again with a different oil thickness or a different maximum and minimum of amplitude modulated voltages.

The dynamic analysis final objective is to establish both the switching on-off time for various thicknesses and also the mathematical physical relationship to Bessel function in chapter 1, section 1.10.

Chapter 3: Results and Discussion

3.1 Introduction

All static experiments were performed on devices with IDT in the range between 80 μm up to 160μm. The IDT were manufactured in the thin film lab as described in chapter 2. Chapter 2 looked at the approach to fabricate the IDT for static experimental characterisation of the device. The objectives of this chapter are to show the results of the static and dynamic experiments. The previous work in this field was limited to a very small amount of static experimental data (Wells 2009).

The previous research on this optical device was part of a study of other possible methods for optical devices which shows the possibility of creating a wrinkle by using Decanol and hexadecane oil as alternative gratings. The previous work included an equation that predicts factors which the wrinkle depends on (see equation 16) and in that equation a scaling relationship with an exponential dependent on film thickness divided by electrode width was not systematically tested. The work on the modelling equation is continuing and a new derivation has shown an agreement with the finding of the previous research. In this systematic research another liquid was used and also various electrodes width with a very thin layer of SU8 was used to examine the modelling relationship which produced a slope of 2π in the previous research. To prove the theoretical model of any relationship, multi linear regression in Excel was used, and each individual experiment was treated as one (x,y) point on a line, which resembles the theoretical model. The error between the fitted mathematical model and the experimental data could be indicated by using the regression error in Excel. The systematic approach is to repeat the process for up to 8 sets of experiments which will be used to populate the Excel graph. This systematic approach was used and the

modelling relationship was verified. The characterisation mainly looked at the wrinkle amplitude when it is sinusoidal vs. the applied ac voltage to the IDT, and to observe the oil surface wrinkle thickness stability, repeatability and reliability under variable dielectrophoresis forces (variable AC voltage) and under a different thickness of Decanol.

The V^2 relationship in equation 16 has been derived to predict the scaling relationship with the wrinkle amplitude, in relation to the film thickness and the IDT electrode width. The main assumptions in deriving equation 16 in chapter 2 are assuming the wrinkle amplitude is smaller than double the electrodes gap, and the profile of the oil undulation is described by Fourier series expansion up to second order only. The oil-air interface for the wrinkle is sinusoidal and the oil-air interface does not change the electric field.

The objective of those experiments is to find a calibration factor which shows that the trend of the theoretical equation agrees with the experimental results. The theory uses assumptions and approximations as close as possible to the mathematical model.

The scaling factor is investigated by rearranging equation 16 to make it as an equation of a straight line in the form

$$\log_e\left(\frac{\Delta h}{V_0^2}\right) = m\left(\frac{h}{d}\right) + C \qquad \text{Equation 17}$$

Equation 17 is used in the static experiments for Decanol oil. The oil thickness was varied from 12 μm up to 40 μm for electrodes gaps between 80 μm up to 160 μm.

In this chapter the experimental results are shown to be in line with the mathematical model with a constant scaling factor for various electrodes width.

3.2 Device IDT fabrication results

A set of ITO covered IDT of electrodes gap (80 μm, 120 μm, and 160 μm) were manufactured and tested, as described in chapter 2, and in order to operate the optical device for static experiment, the method in Chapter 2 was used to produce 36 IDTs with electrode gap (80 μm, 120 μm, 160 μm). For the dynamic experiments, a set of IDT were manufactured with electrodes, gap width from 5 μm up to 40 μm as shown in figure 17 to figure 20.

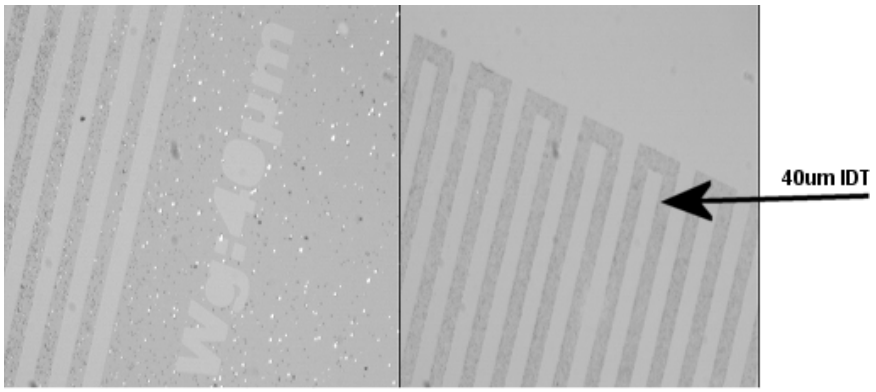

Figure 17 40µm IDT without SU8

Figure 18 10μm IDT without SU8

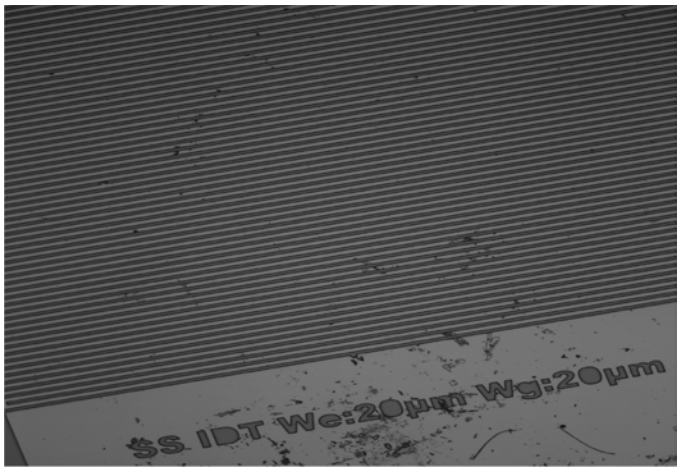

Figure 19 20μm IDT without SU8

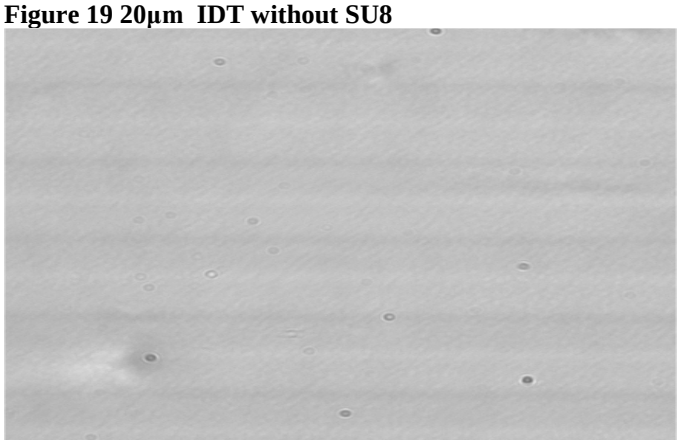

Figure 20 40μm IDT with SU8

3.3 Static experiments analysis results for 120μm

The IDT of 120μm electrodes gap was used to scale the model in equation 17; and table 2 shows the IDT data.

Sample name	120 w211091204
ITO	100 ohm/m^2
Dielectric layer SU8	0.5 μm
Electrode width/gap	120 μm
Electrode pitch	240 μm
Oil Material	Decanol
Wavelength	6.33E-07 m

Table 2 Optical device tag for static experiments

The following guideline was followed in obtaining the experimental results. The IDT batch in table 2 is identified by a sample name, that starts with the electrode gap width i.e. 120 is 120μm which is the electrodes width, after the electrode width is the date of manufacturing i.e. 21109, and followed by the experiment number on that date which was selected for analysis i.e. (4) in the table 2. Each experiment is a set of 11 various incremental voltages which is combined with the image of the wrinkle amplitude at that voltage. The image of the thickness at the start of each set of voltage/wrinkle amplitude is analysed and the images were converted from pixel to micrometre, as shown in section 2.6.1.

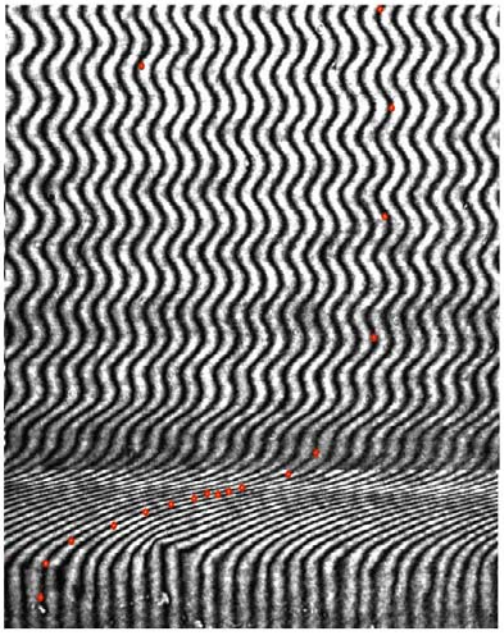

Figure 21 Edge interferometer image for 27.7µm thickness

The applied incremental r.m.s. voltages were observed between 88V (rms) and 292V (rms) as shown in figure 23 and figure 24. The recorded pixels in the wrinkles' interferometer images were then converted to micrometres, as shown in the method described in chapter 2 section 2.5. The amplitude of the wrinkles was plotted against the V^2 of the above applied voltages, which shows that the amplitude of the ripple under voltage is proportional to V^2. It indicates that the Decanol oil has spread over the whole electrode area on the surface of the IDT sample and also the wrinkle's amplitude of the Decanol oil is linearly varied according to the V^2 relationship. This process was repeated for various thicknesses, figure 21 and figure 22 show a sample of measuring two thicknesses of 27.7µm and 14.6µm respectively.

Figure 23 and figure 24 were used to see the V^2 relationship (first regression) and it is also clear from figure 25 that there is an accurate V^2 relationship with the wrinkle amplitude with a very small error. Figure 26 shows the modelling relationship in

equation 17 for the mathematical model follows the experimental fitted data for 120µm electrodes width device. This part of the static experiment proves that the wrinkle is an undulation, which varies linearly with V^2. The V^2 follows the model for that set of electrodes, in this case 120µm. The experimental results and the second regression model are in an acceptable residual error of 78% as shown in figure 26.

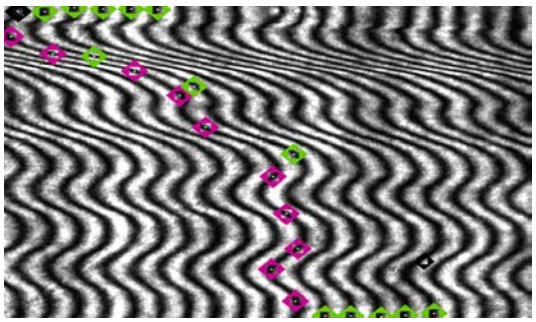

Figure 22 Edge interferometer image for 14.6µm thickness

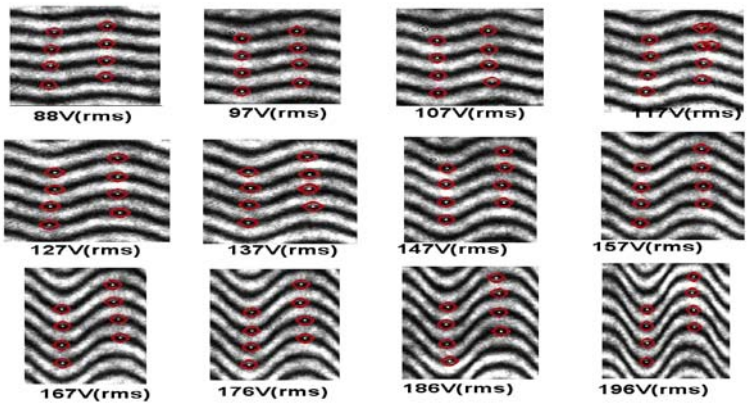

Figure 23 Wrinkle amplitude Interferometry images from 88 V (rms) to 196 V (rms)

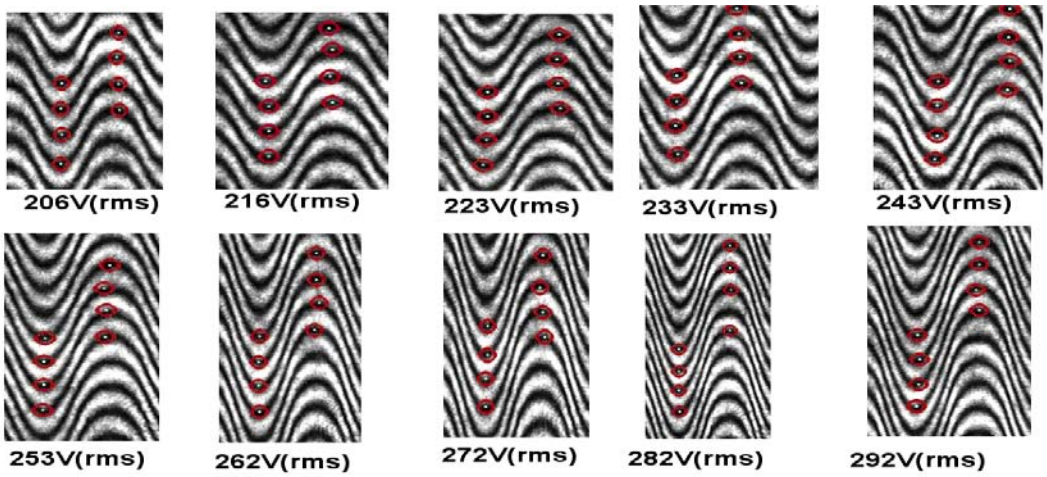

Figure 24 Wrinkle amplitude variations as the ac voltages increase from 206 V (rms) to 292 V (rms)

Figure 25 and figure 26 show that the 8 static experiments for 8 different Decanol oil thicknesses follow a linear relationship.

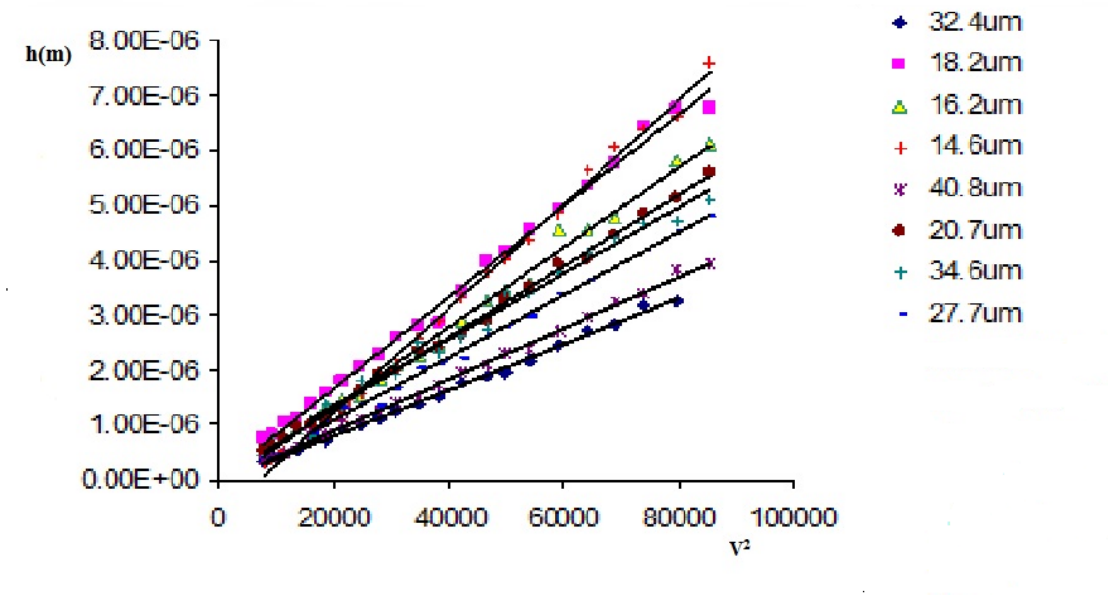

Figure 25 Wrinkle amplitude h(m) vs. the applied voltage square

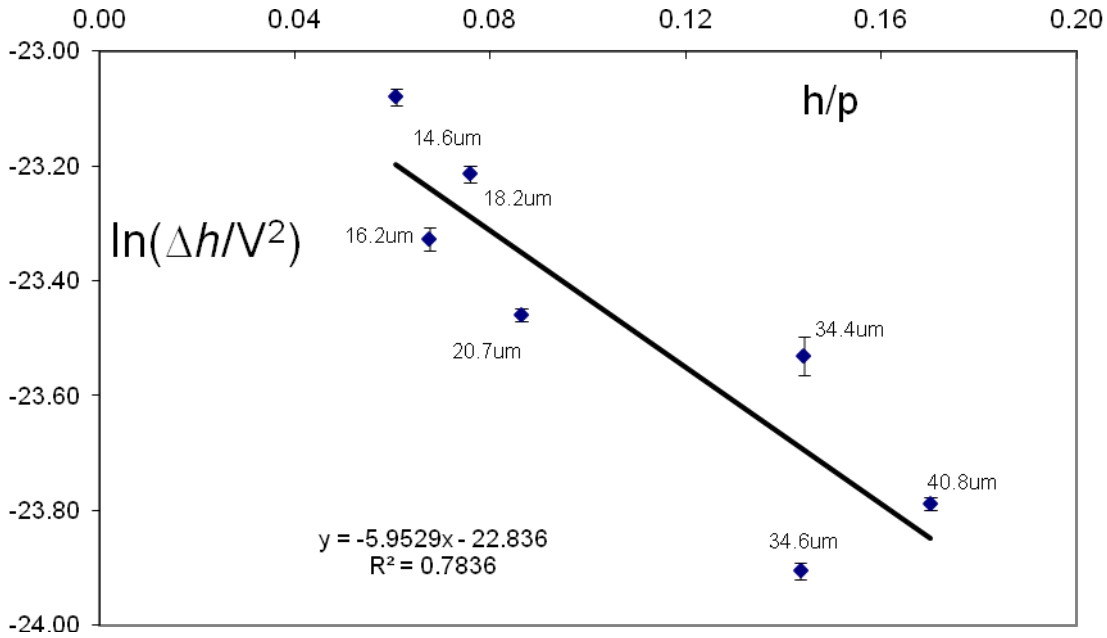

Figure 26 the second regression for 120μm optical device model verification

3.4 Experimental results for 80μm and 160μm

The static experiments of 120μm were extended to optical devices of 80μm and 160μm.The purpose of this section is to examine if the V^2 modelling relationship is related to the wrinkle amplitude and also to examine if the mathematical model of equation 16 scales to the experimental results and identifies some of the errors.

3.4.1 Static results for 160µm electrodes

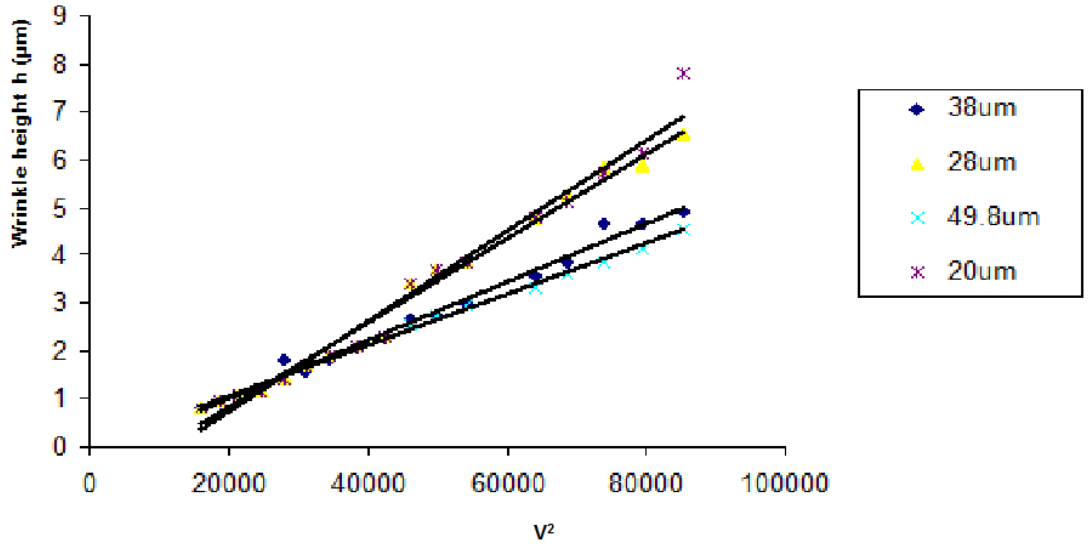

Figure 27 Wrinkle height vs. the square of the applied voltage for 160µm for 4 oil thicknesses

Figure 27 shows the relationship between the applied AC Voltage (V^2) with relationship to the surface wrinkle amplitude (µm) for various oil thickness for 20µm, 28µm, 38µm and 49.8µm.

The second regression of figure 28 shows the mathematical modelling approximation of various factors of the modelling relationship of equation 16 compared to the experimental data obtained from the set of the experiments for 160µm size of electrodes width.

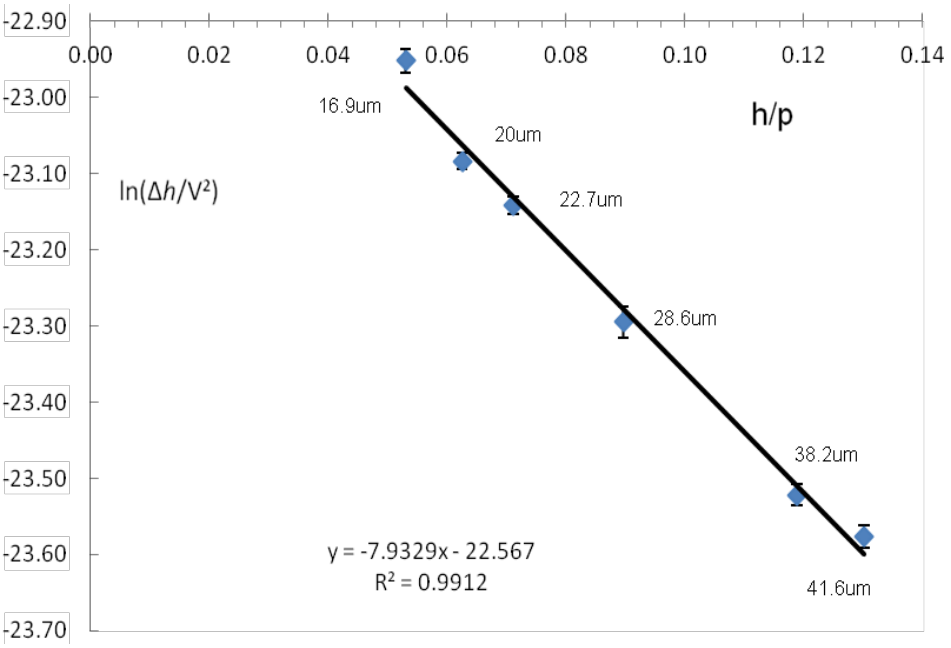

Figure 28 the model (second regression) for 160µm optical device model verification for gradient vs. the changes of thickness over the pitch of the electrodes obtained from the first regression

3.4.2 Static results for 80µm electrodes gap

Figure 29 shows the relationship between the applied AC Voltage (V^2) with relationship to the surface wrinkle amplitude (µm) for various oil thickness for 18.8 µm, 26.8 µm, 29.3 µm and 35.5 µm.

The second regression of figure 30 shows the mathematical modelling approximation of various factors of the modelling relationship of equation 16 (second regression) compared to the experimental data obtained from the set of the experiments for 80µm electrodes width.

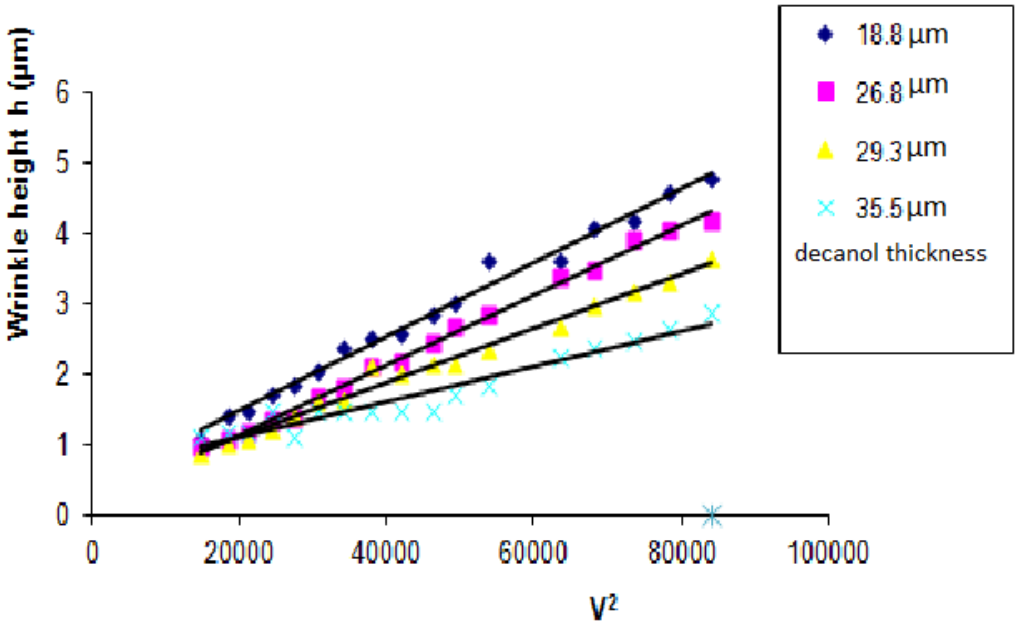

Figure 29 Variation of applied voltage squared with the Wrinkle amplitude for 80µm electrodes gaps

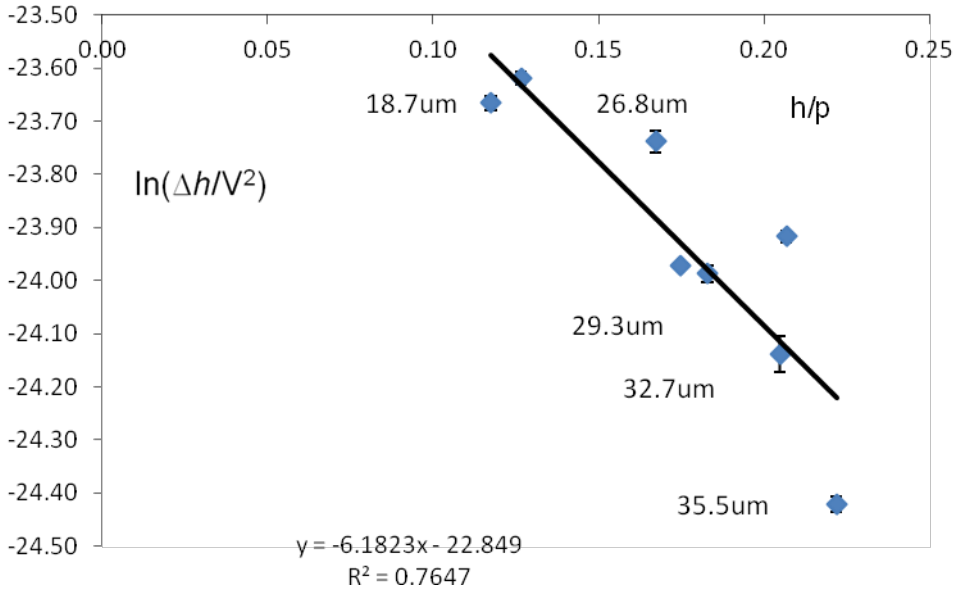

Figure 30 Second regression model for 80µm experimental data

All the data obtained from 80µm, 120µm and 160µm are fitted for the regression line which represents the mathematical model approximation to the experimental data for various electrodes gap, as shown in figure 31.

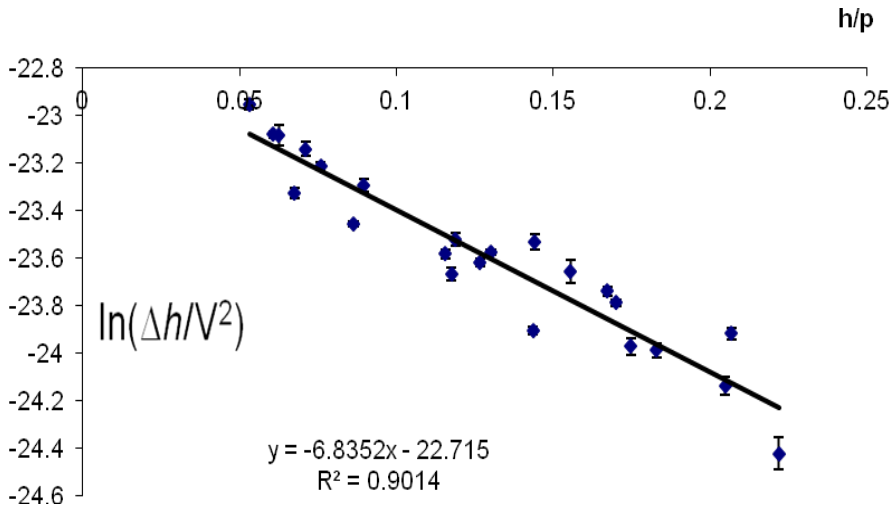

Figure 31 Regression model for all the data obtained from 80µm, 120µm, and 160µm

3.5 Uniformity of Decanol Oil

The uniformity of the Decanol oil was tested for the variations of thickness under different voltages (97-290) V. This experiment shows that there is an error in the thickness of oil (*h*) which needs to be estimated and included in the static analysis of section 3.1 and 3.2. Figure 32 is used to generate the errors in the regression model. Figure 32 is generated by changing the voltage that is applied to the Decanol oil and observing the thickness height variations in pixels across the surface of the electrodes, it is noted that there is little error on the thickness of the Decanol oil when the voltage varies between 97v (rms) to the highest voltage that is applied to the oil at 290v (rms).

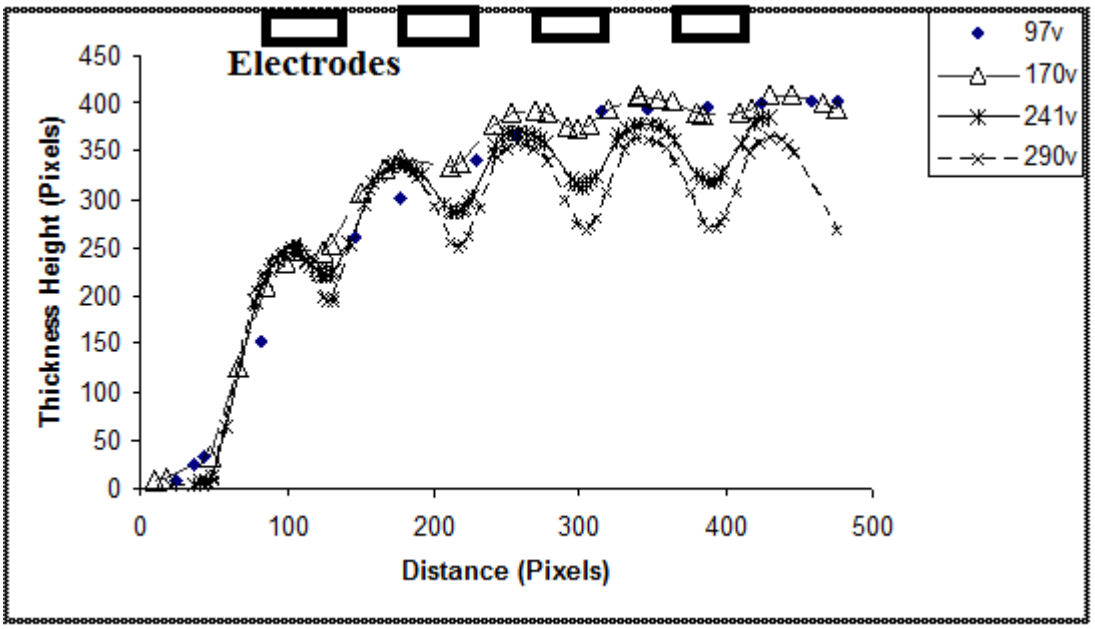

Figure 32 Decanol oil thickness variation across the electrodes with four different applied voltages

3.6 Other types of oil static verifications

In this section the static experiment procedures in the previous sections were repeated in order to test the relationship in equation 17. Equation 17 is used again here to test the variation of the wrinkle amplitude Δh with different oil material parameters. The procedure in chapter 2 was used with 80µm electrodes pitch and the oil was changed from 1-Decanol to 1-Octonal, 2-Octanol and paraffin. The ac voltage at 20 kHz is increased from 100V rms to 300V rms for the amplitude of the wrinkle. The amplitude is measured at peak and measured at trough as shown in chapter 2. The initial voltage was raised to 680 volts rms at 20 kHz to spread the oil (1-octanol, 2-Octnol and Paraffin). The results for amplitude variation under various thicknesses of oil are plotted against V^2. As shown, those steps were repeated for oil thicknesses for each IDT of electrodes pitch of 80µm. Figures 33 to Figure 39 show the results for 1-

Octanol, 2-Octanol and Paraffin. The procedure in chapter was repeated with the material properties value of those three oil were used in equation 14 and equation 17

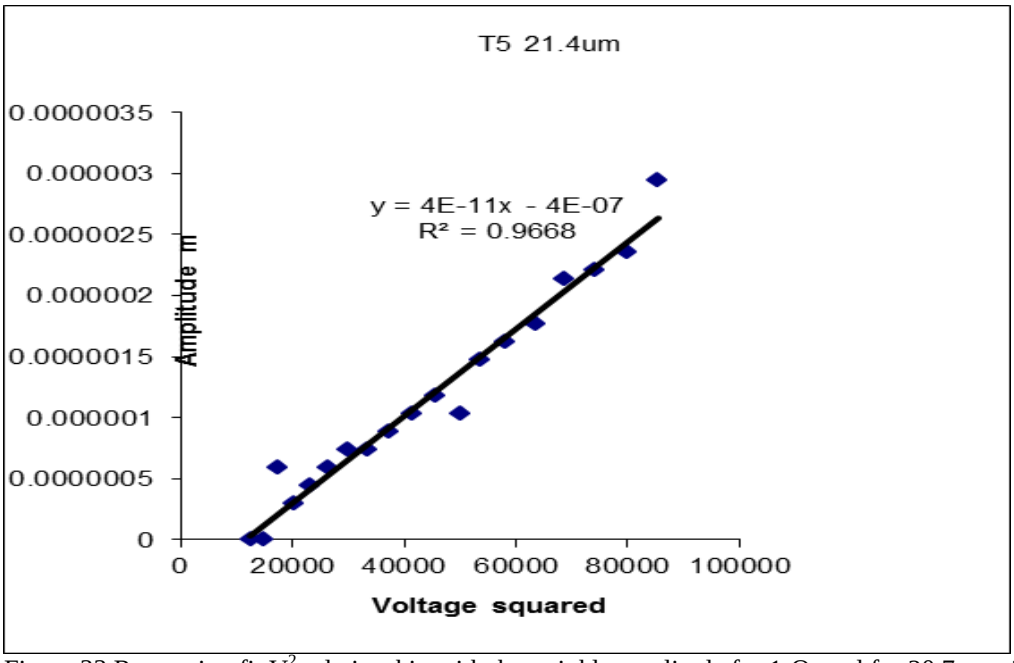

Figure 33 Regression fit V^2 relationship with the wrinkle amplitude for 1-Octnol for 20.7µm oil thickness

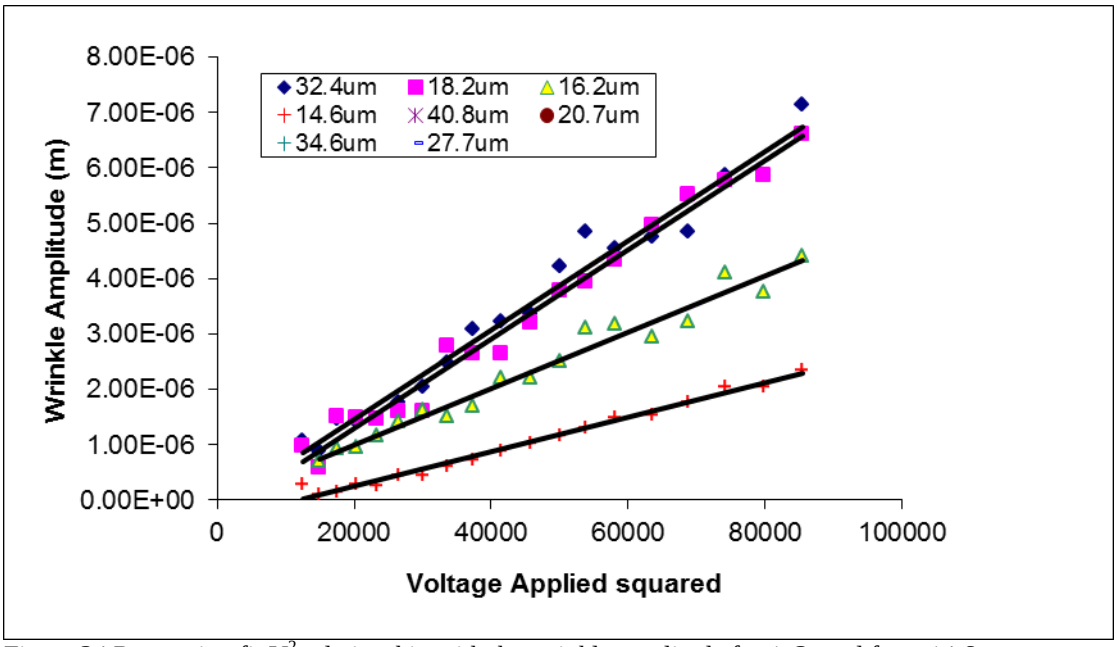

Figure 34 Regression fit V^2 relationship with the wrinkle amplitude for 1-Octnol from 14.6µm up to 40.8µm oil thickness

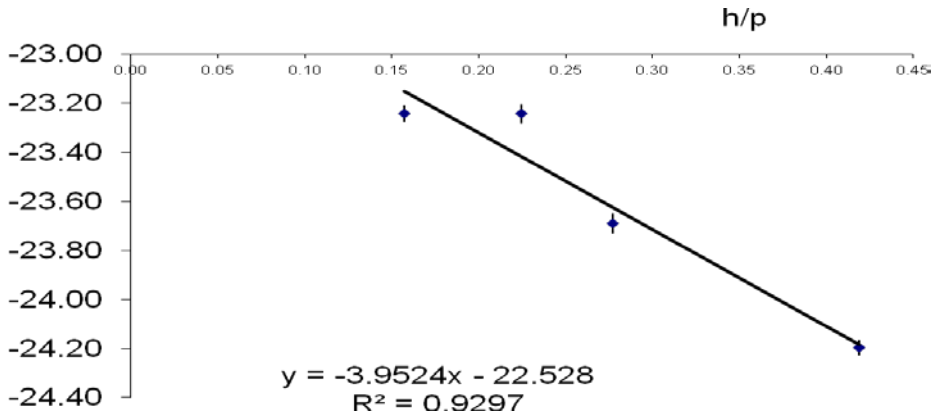

Figure 35 the second regression for 1-Octanol for optical device model verification

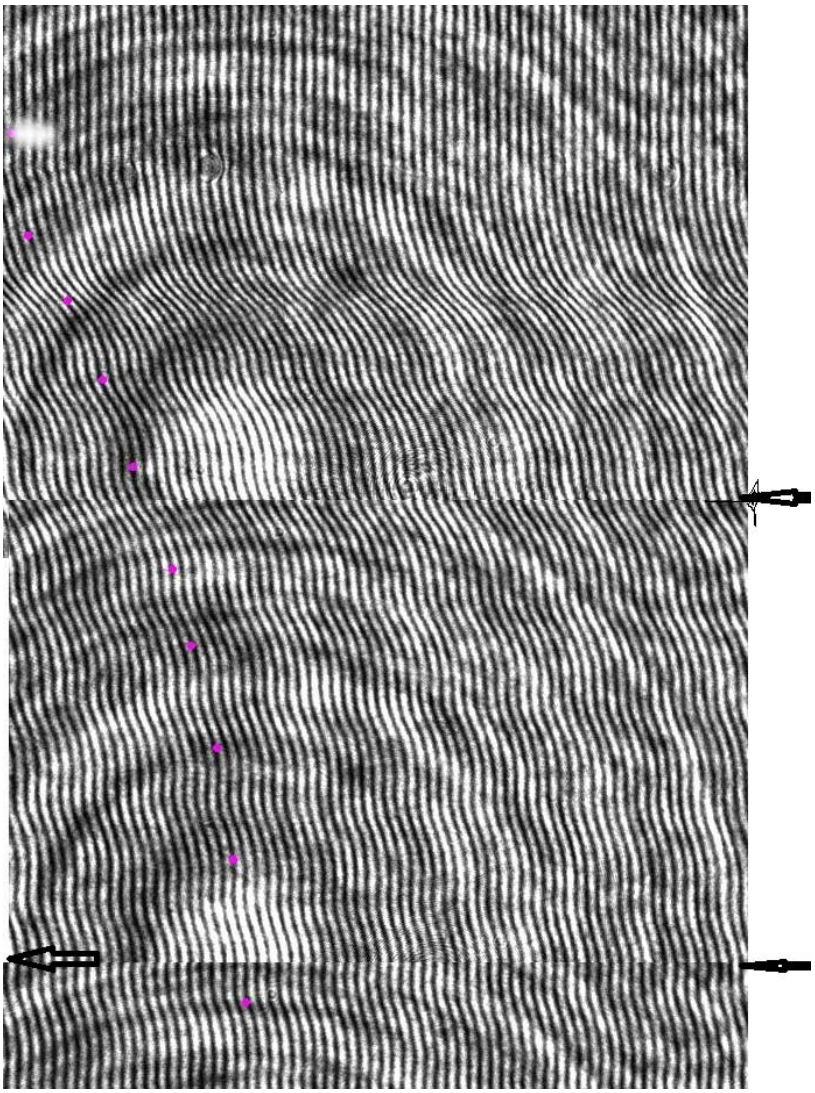
Figure 36 Thickness pictures for 2-Octnol

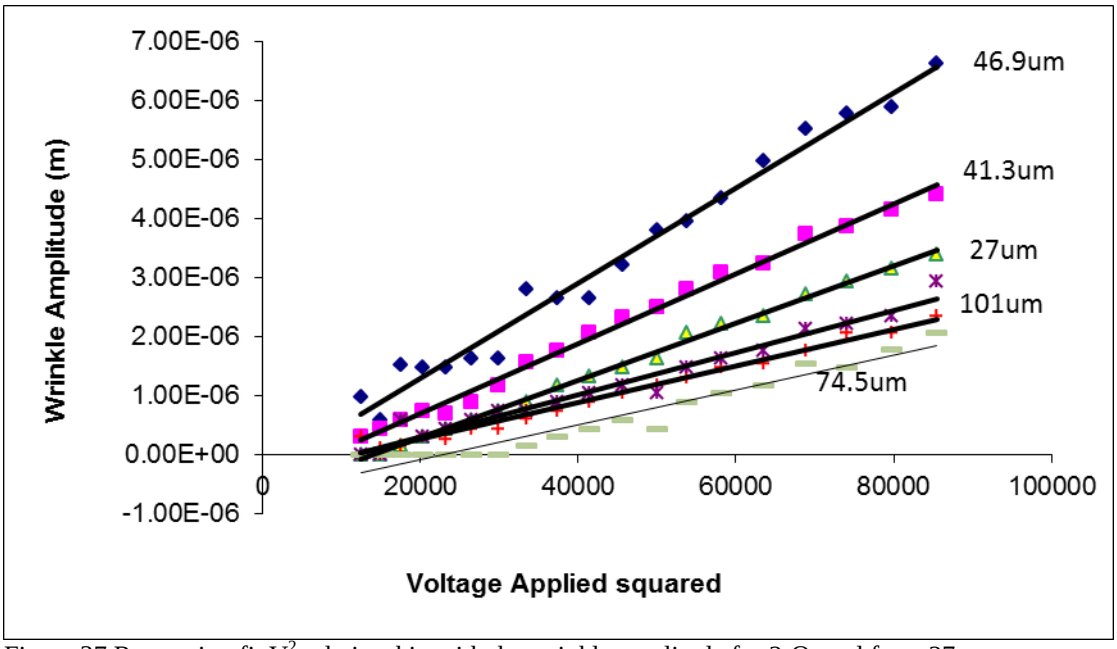

Figure 37 Regression fit V^2 relationship with the wrinkle amplitude for 2-Octnol from 27µm up to 101µm oil thickness

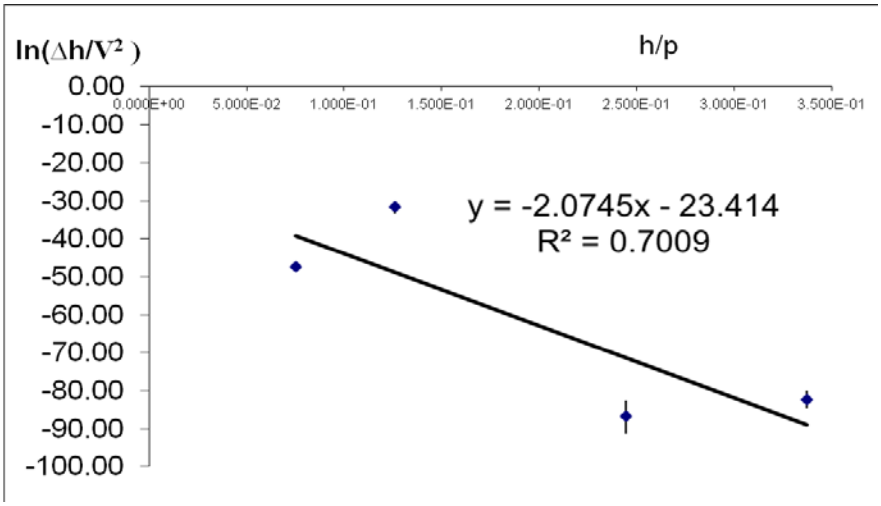

Figure 38 the second regression for 2-Octanol for optical device model verification

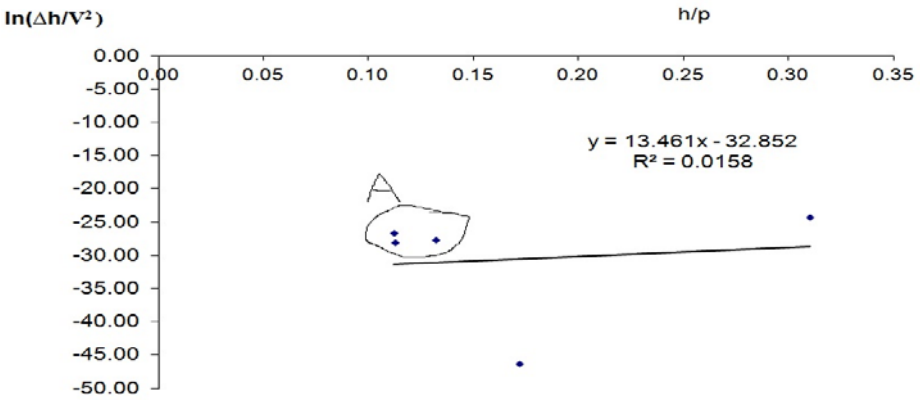

Figure 39 the second regression for paraffin oil

3.7 Dynamic studies

The dynamic studies required a new batch of electrodes, with smaller electrode gaps than the IDT electrodes, which were used in the static studies i.e. 10μm pitch (5μm electrodes spacing), 20μm pitch (10μm electrodes spacing), 40μm pitch (20μm electrodes spacing), and 80μm pitch (40μm electrodes spacing). The static experiments' results showed that Decanol oil has a sinusoidal profile (see section 3.5). The aim of the dynamic study is to relate the V^2, the height of wrinkle that was shown in the static analyses to a more practical use of switching and the intensities of the diffraction spots to the physics' theory and use that idea to find the switching time of those diffraction spots for various applications. To achieve this objective, firstly the variation in the amplitude (height) of Decanol oil needs to be measured across the electrodes with minimum and maximum voltages (triangle shape waveform Figure 44), and secondly the switching on and off time of the zero order, first order and second order. The experiments on the dynamic studies preliminarily results are shown in this chapter, the first results of the experiment is, a device of 80μm pitch (40μm electrodes spacing) interdigitated electrode (IDT) and also results on 40μm pitch (20μm electrodes spacing) are shown. The first objective is to set the voltage to the maximum and minimum so that those voltages create the wrinkle amplitude in the surface of the Decanol oil, secondly the effects of those wrinkles on the switching time characteristics of the device. Further experiments was carried out on devices of interdigitated electrodes of width 40μm pitch (20μm electrodes spacing) and 20μm pitch (10μm electrodes spacing). In all those experiments only Decanol oil was used in all the devices. The experiments that were carried out using the dynamic switching

of the amplitude of the Decanol oil surface wrinkle at 20µm and 40µm electrode spacing periods showed promising results. The dynamic switching was investigated by monitoring the time dependent intensity of the zero, first and second diffracted orders by adding another 543nm green laser and a photo detector to the optical path of the static experiment as it is shown in the dynamic part of the experimental set up in Figure 40 and Figure 41 of the photograph and also the block diagram of Figure 42 of the experimental set up. In those figures a green laser and light photo diode are inserted in position 17, 10 and 18 that show the diffraction patterns intensities in Figure 41 and Figure 42.

3.8 Dynamic experiment results

There are three important parts to the dynamic experiments and those are thickness measurement, diffraction pattern efficiency (Bessel agreements), and switching time. The experimental set up picture is shown in Figure 40, the dynamic part is extracted and shown in Figure 41, in this figure a green laser was inserted the location 17, photo diode in location 10 and a step motor was used to move the light detector between the diffraction spots in location 18. Other locations in Figure 40 and Figure 41 can be summarised in the block diagram of Figure 42.

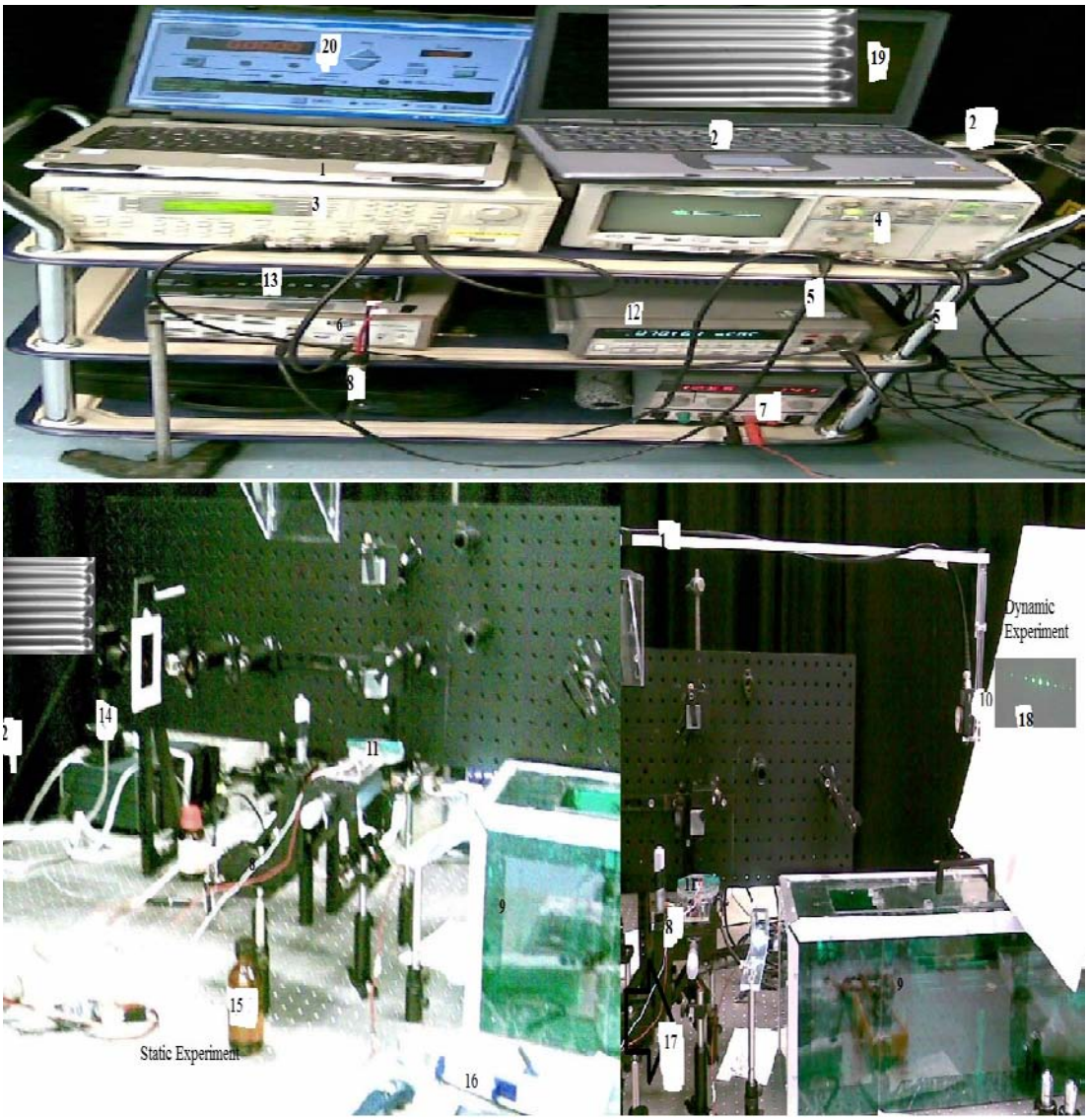

Figure 40 dynamic and static experiments set up

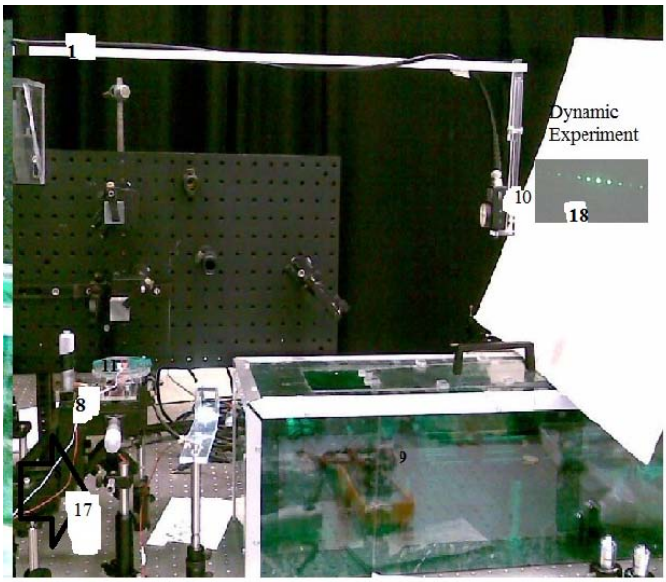

Figure 41 The dynamic part of the experimental set up extracted from Figure 40

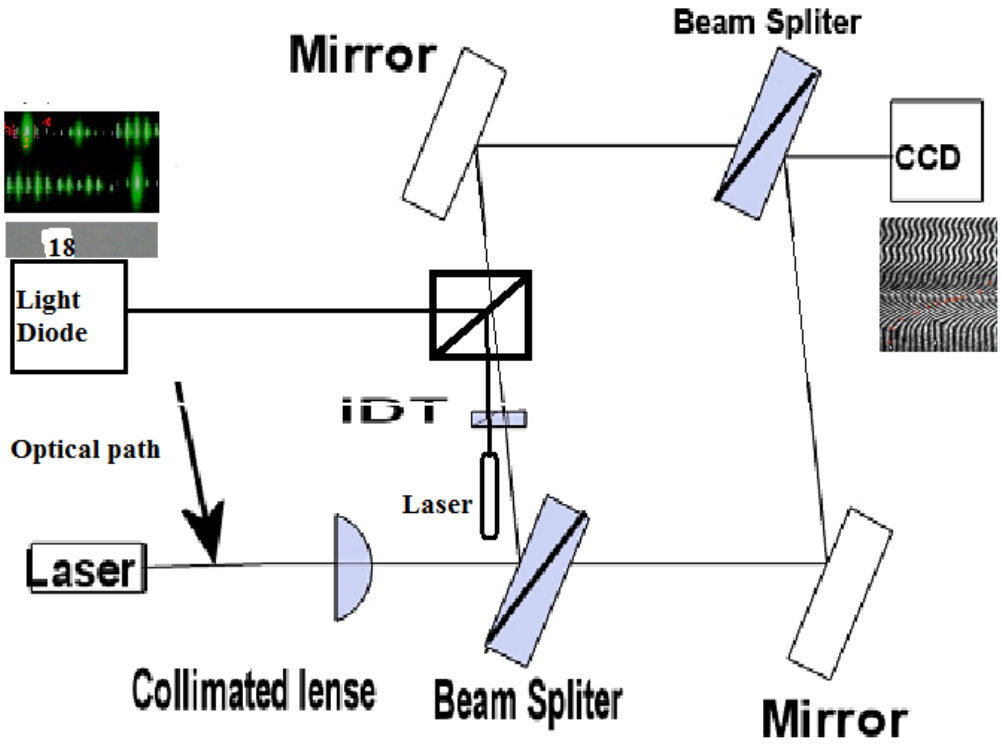

Figure 42 Dynamic and static experiments block diagram

In the dynamic experiment, the static experiment is used to measure the thickness of the Decanol oil and to plot the Bessel function that is the relationship between the voltage applied and the photo diode intensity voltages for zero, first and second orders.

The dynamic experiment uses green laser that transmits into the device (IDT) , beam splitter to direct the laser beam into DT36A Thorlabs light photo diode detector. In Figure 41 and Figure 42 the light diode detects the diffraction pattern displayed in position 18 and it is connected to the two channels oscilloscope (Agilent S4622A) as shown in position 10 in Figure 41.

3.8.1 Thickness measurement

The procedure in chapter 2 was applied and the Decanol oil thickness was measured using the interferometer images at the start of the experiment and at the end of the experiment, as shown in Figure 43 Decanol oil thickness for 40µm electrodes width over 2 hours of use Figure 43 Decanol oil thickness for 40µm electrodes width over 2 hours of use shows that the oil thickness at the start of the experiment was approximately 8.7 μm with 6 fringes shifted from the area outside the electrical field. At the end of the experiment (second order switching data capture), the oil thickness dropped to only 4 fringes shift (5.80 μm).

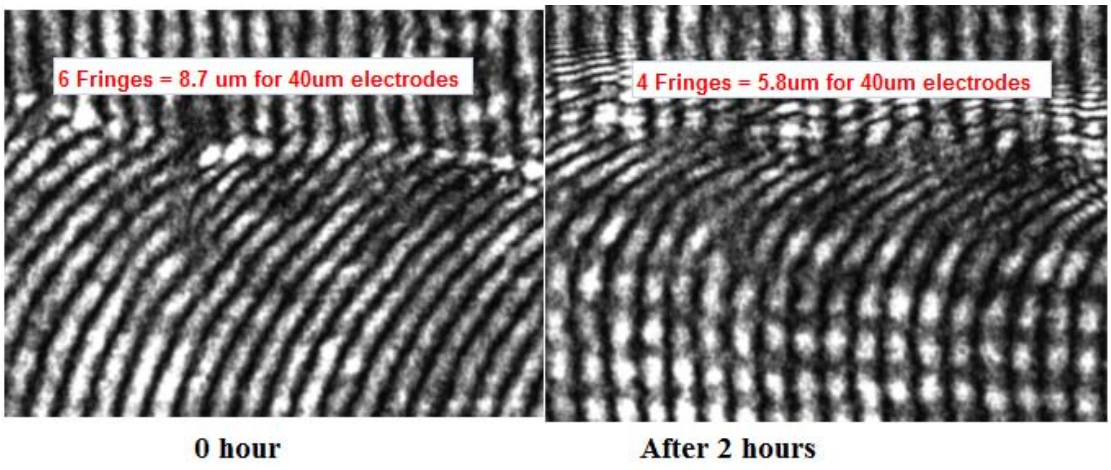

Figure 43 Decanol oil thickness for 40µm electrodes width over 2 hours of use

3.8.2 Signal voltage for Decanol oil

The signal voltage is used to generate the wrinkle that is used to produce the various diffraction orders (zero, one and two). The signal voltage is found from the static study of the Decanol oil to be between 87.5 volts (rms) and 306v (rms). This range of voltage will generate zero, first and second diffraction orders. Figure 44 shows the relationship of the triangular voltage that is fluctuating between 87.5 v (rms) and 306v(rms) with zero order, it clearly shows that when the signal voltage is at minimum the zero order is at maximum. The device that is used to generate the zero, first Figure 45, and second order Figure 46 was 40µm electrode spacing (80µm pitch). The thickness of Decanol oil started in Figure 45 at 8.7µm and thinned down to 5.8µm after 2 hours of subjecting the Decanol oil in the device to the signal voltage in Figure 44.

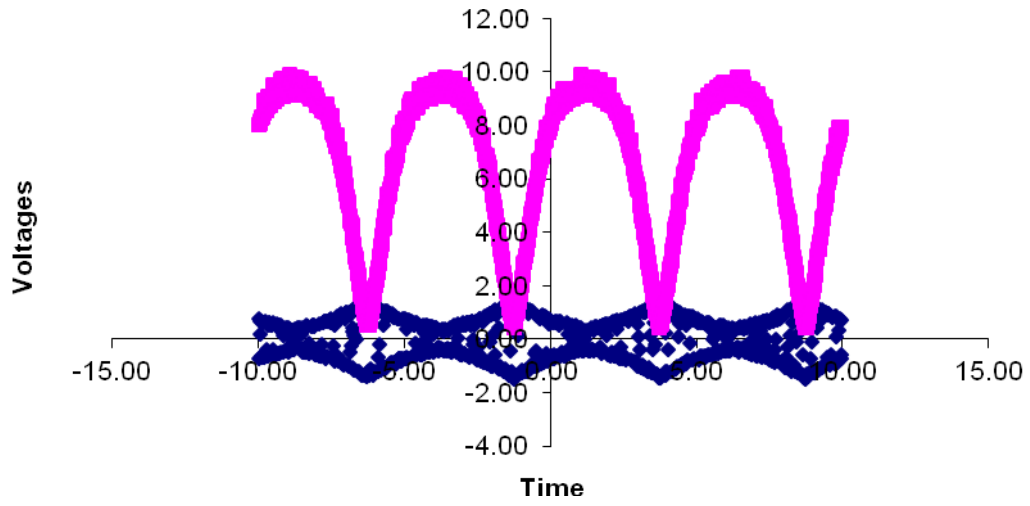

Figure 44 The relationship between the signal voltage (scale x150) and the voltage intensity for zero order for 40um device with 2um SU8

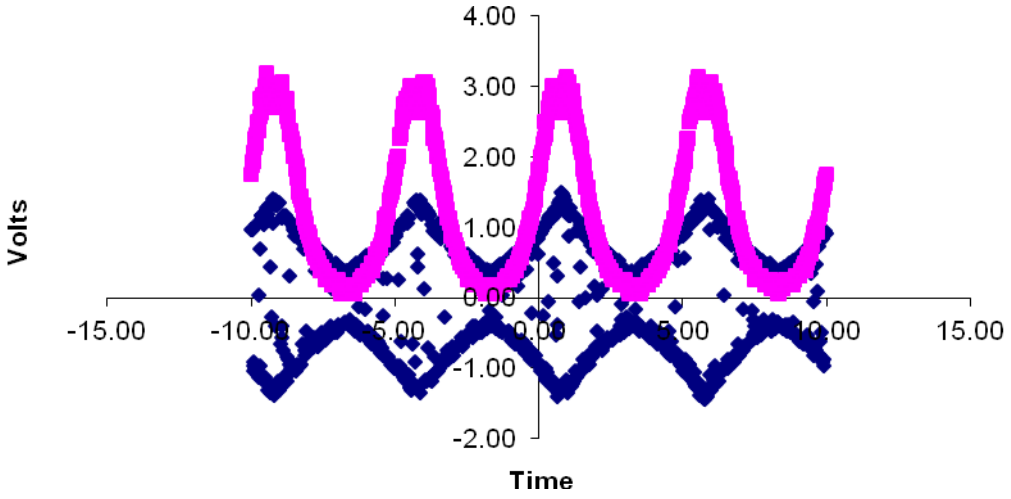

Figure 45 the relationship between the signal voltage (scale x150) and voltage intensity for first order for 40um device with 2um SU8

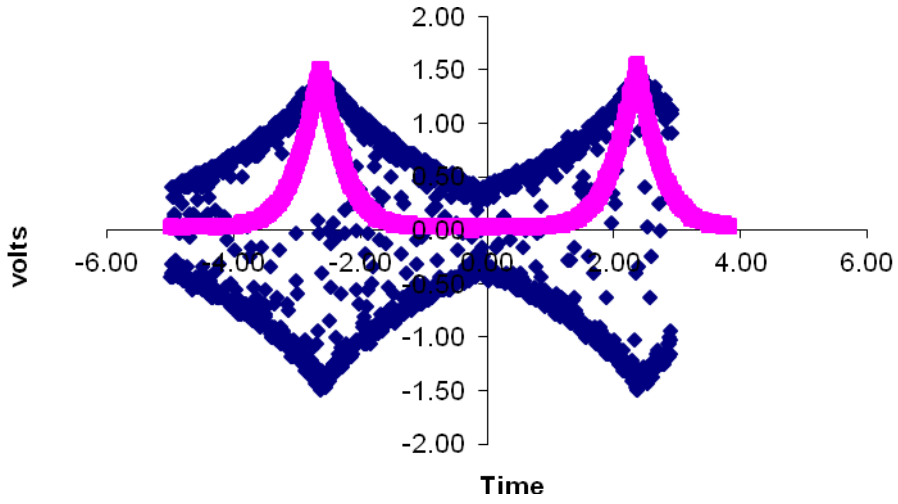

Figure 46 the relationship between the signal voltage (scale x150) and voltage intensity for second order for 40um device with 2um SU8

3.8.2 Bessel behaviour of the Undulation

The signal voltage vs. time and photo diode (Pd) intensity voltage vs. time (Figure 44, Figure 45, Figure 46) were used to obtain Bessel function behaviour (equation 8) by modulating the voltage with triangular waveform. The Bessel diagram of the intensity of the zero order, first order and second order has a Bessel relationship to the applied signal voltages to the electrodes of the 40µm device, as shown in Figure 47 that shows the Bessel relationship of the variation of the intensities of zero, first, and second orders with ac signal input voltage between (87.5v-306v) rms using 40um device. The intensities of the photo diode are shown to confirm the switching of the photo diode between various intensities that is related to the signal voltage waveform applied to the 40µm device.

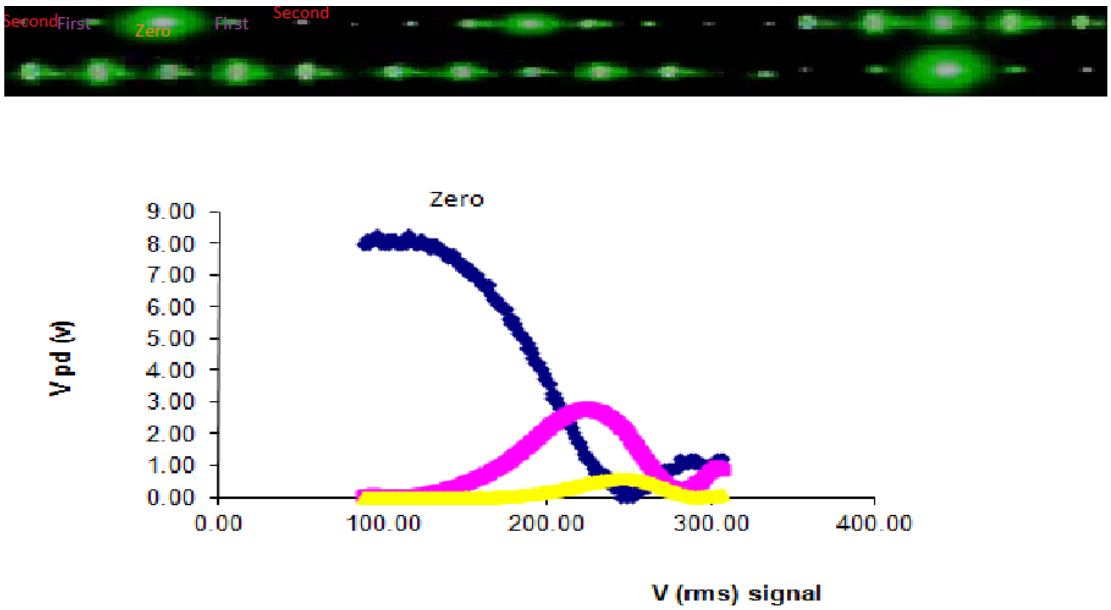

Figure 47 Bessel relationship that show the variation of the intensities of zero, first, and second orders with ac signal input voltage between (87.5v-306v) rms using 40um device

The procedure that was followed to generate the variation of the intensities that is shown in Figure 47, is first to set the maximum and minimum signal voltages that can generate a wrinkle which will create the zero, first and second orders in the photo diode light intensity from that is related to the voltage applied to the photo diode. After achieving the maximum and minimum voltages the modulating waveform is switched to a square wave with the values of the maximum and minimum voltages found in the first step. The second step requirements is to have oil thickness and properties so that it can undulate and provide wrinkles that create the diffraction orders (zero, first and second) and supply the photo diode with enough voltage sensitivity so that it can detect the green laser diffracted light. Figure 47 shows the relationship between the signal voltage (the voltage that creates the wrinkles) and the intensities of zero, first, and second, the higher the diffraction order intensities voltages the higher the signal voltage, to achieve the second order diffraction order it is required 306v (rms) with nearly 9 volts photo diode intensity, a low serial diode resistance required to be connected with the photo diode to achieve that relationship. This relationship characterises the oil under test for its dynamic Bessel function and it has shown a resemblance to the physics that is shown in section 1.11.2. The photo diode DEM36A was chosen with rise times as fast as 1 nano second.

3.8.3 Switching time calculations

The modulating signal is changed to square wave of 20 kHz with 0.1-20 Hz amplitude modulation as shown in figure 48 and figure 49. The modulation ratio between V_{max} and V_{min} was kept constant. The switching of the thin layer of Decanol was switched for the zero order, first order and the second order of the diffracted spots. Figure 50

shows the way the switching time was calculated for 20µm device and 40µm device in section 3.8.4.

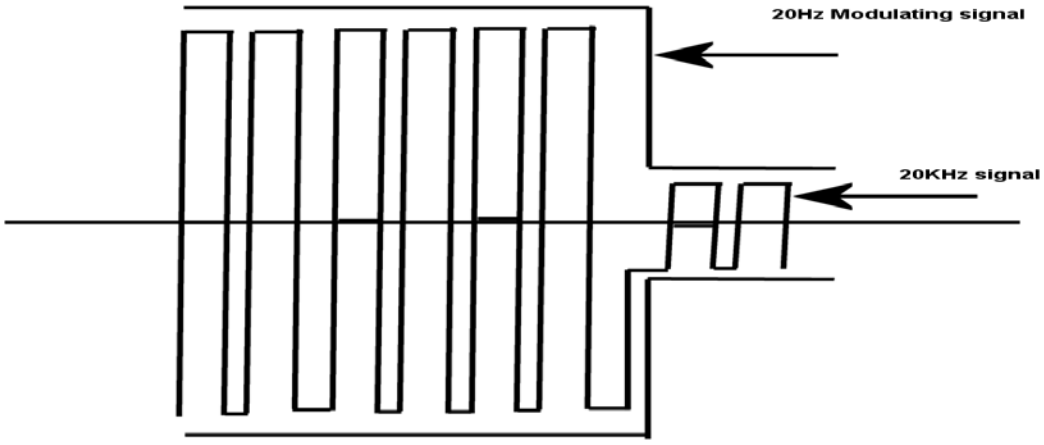

Figure 48 switching off modulated square wave signal voltage

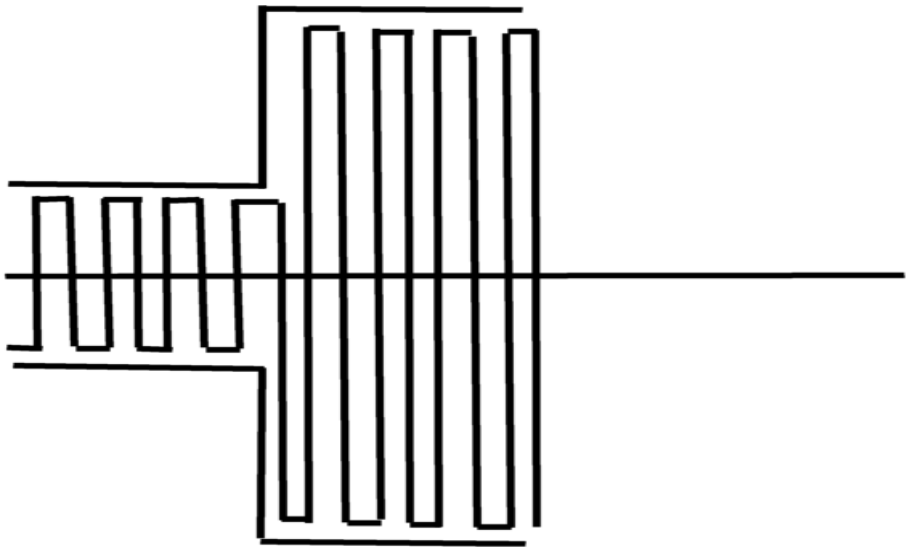

Figure 49 switching on modulated square wave signal voltage

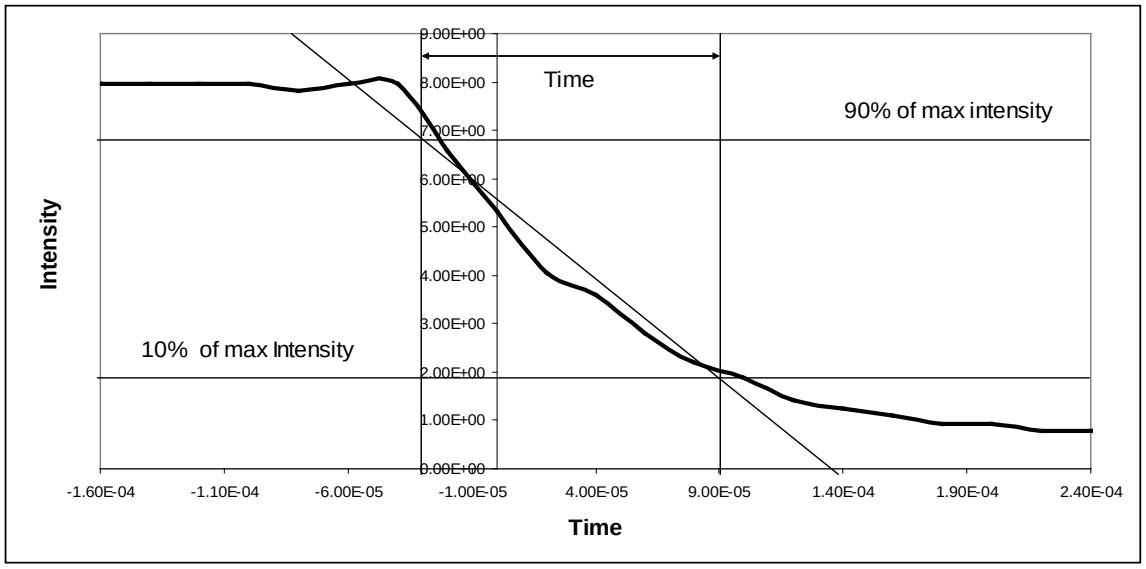

Figure 50 Manual diagram of estimating the switching time of the diffraction spot intensity

3.8.4 Switching time results for 20µm and 40µm electrodes devices

The procedure of section 3.8.3 is used to extract the switching times from the results of capturing the switching the photo diode for 20µm and 40µm. For 20µm device the results are shown in, Figure 54, Figure 55, Figure 56, Figure 57 and for 40µm device are shown in Figure 51, Figure 52, Figure 53, Figure 58, Figure 59, Figure 60, Figure 61, Figure 62, Figure 63 devices for zero, first and second diffraction orders. Table 3 summarise the results for the extracted switching times. Several devices with 10µm, 20µm were damaged because of the high voltage of nearly 300 volts (rms) at 20 kHz and with the modulation of 20 Hz that made the devices easy to be damaged especially with the thin layer of SU8.

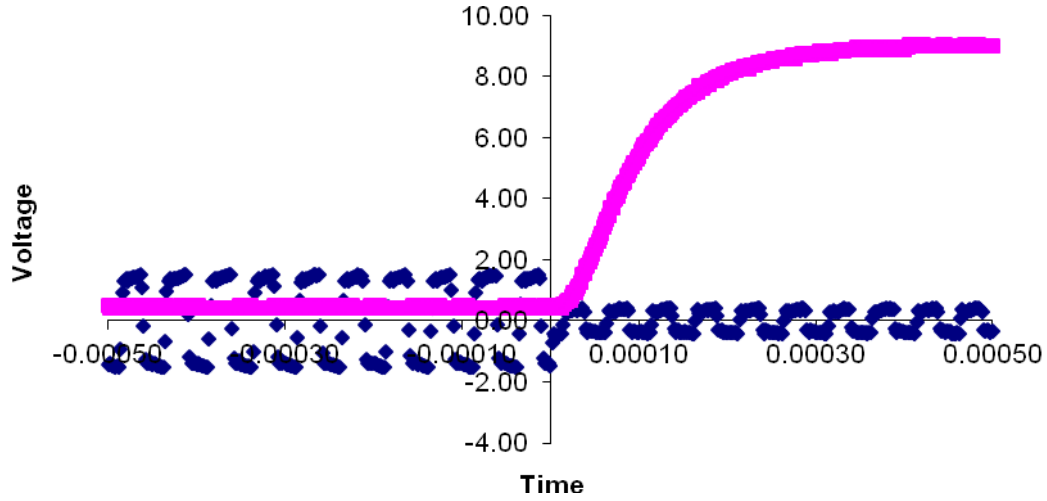

Figure 51 switching response time for 40 um device for zero order photo LED diode intensity voltage in response to the zero signal voltage x150 rms) (140µs switching on)

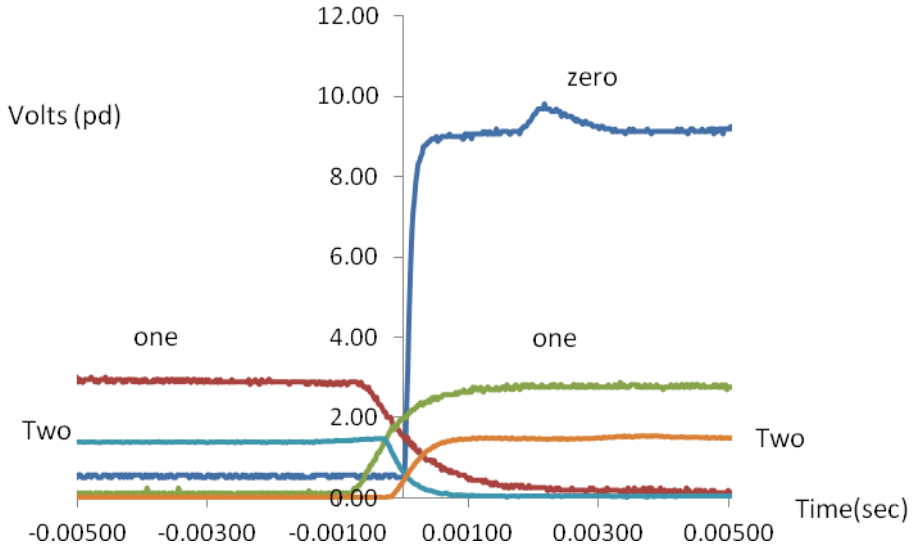

Figure 52 the relationship of the switching response time and the intensity voltages of zero, one and second orders for 40µm device 8.7µm Decanol thickness

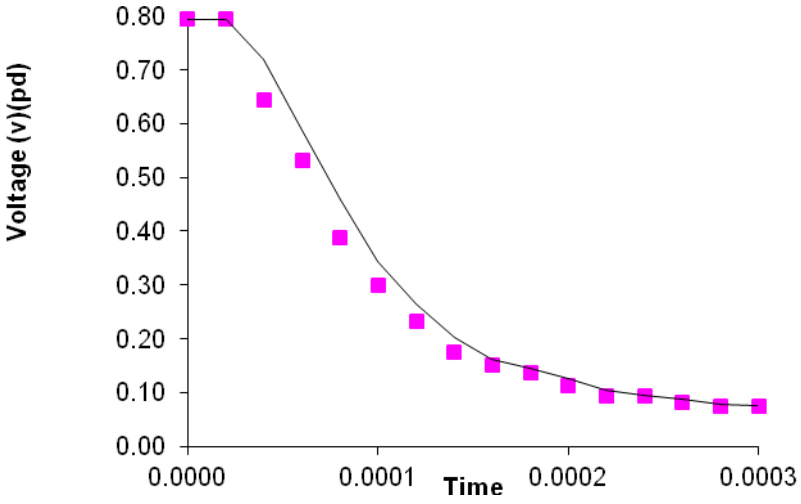

Figure 53 Photo diode switching off response to signal voltage for zero order (220µs) 40µm device.

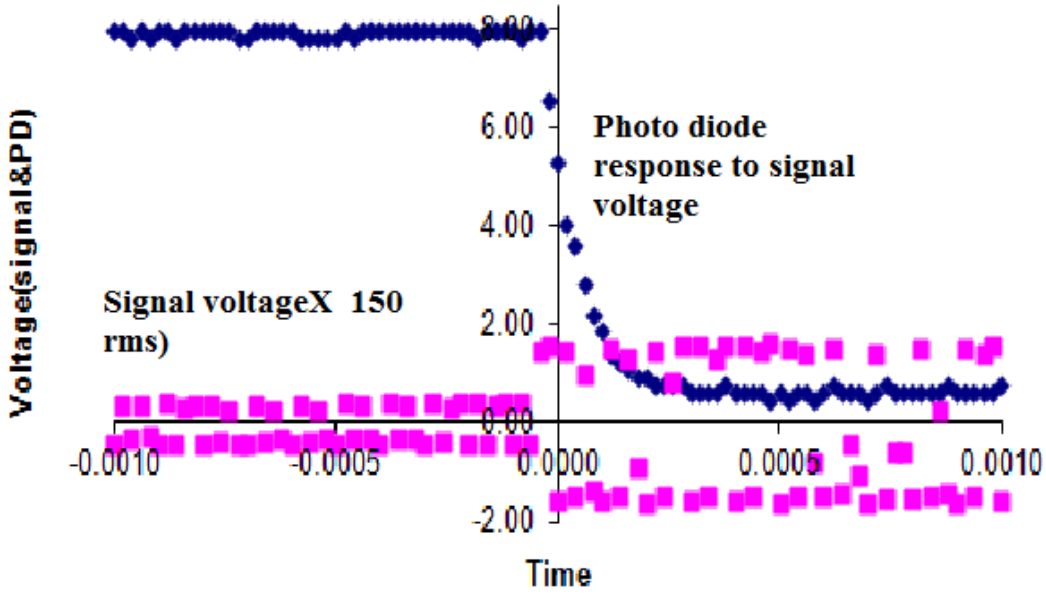

Figure 54 the zero order signal voltage switch off to the 4.35µm oil thickness with 20µm device with the switch on response of photo diode (pd).

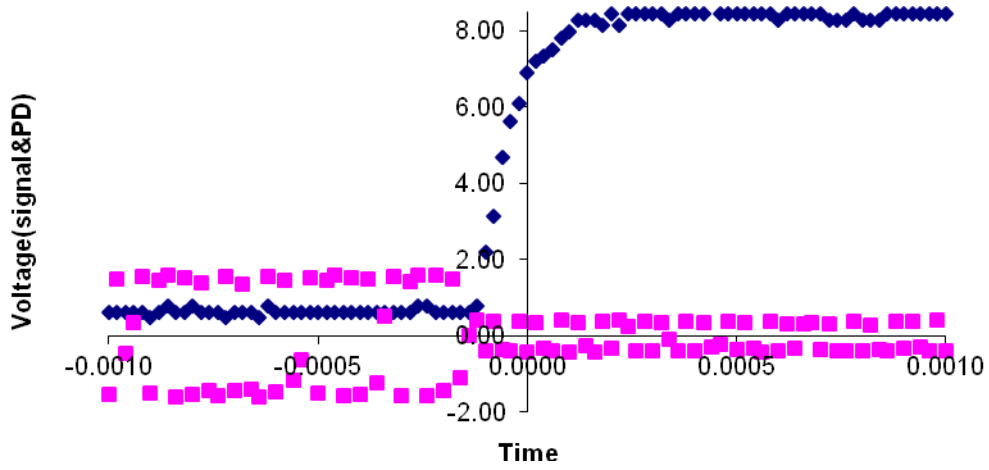

Figure 55 the zero order signal voltage to the 4.35µm oil thickness with 20µm device with the switch on response of photo diode (pd)

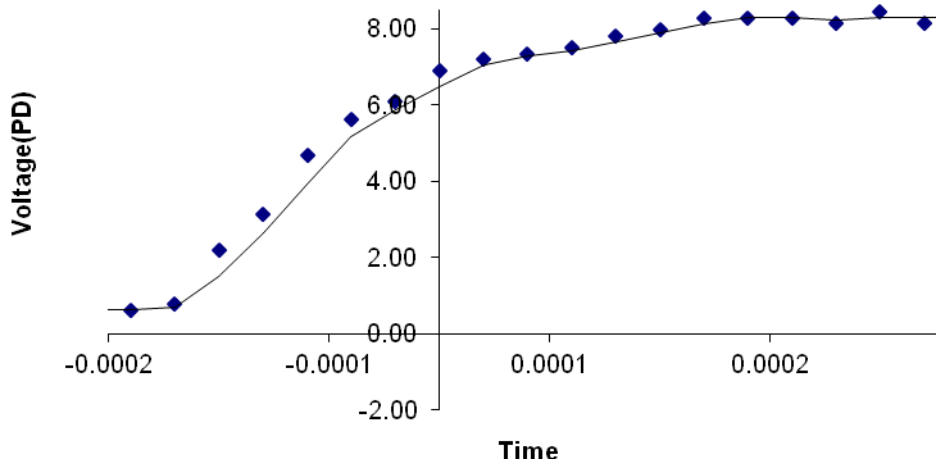

Figure 56 Zero order photo diode switching on extracted from figure 57 for 20µ electrodes

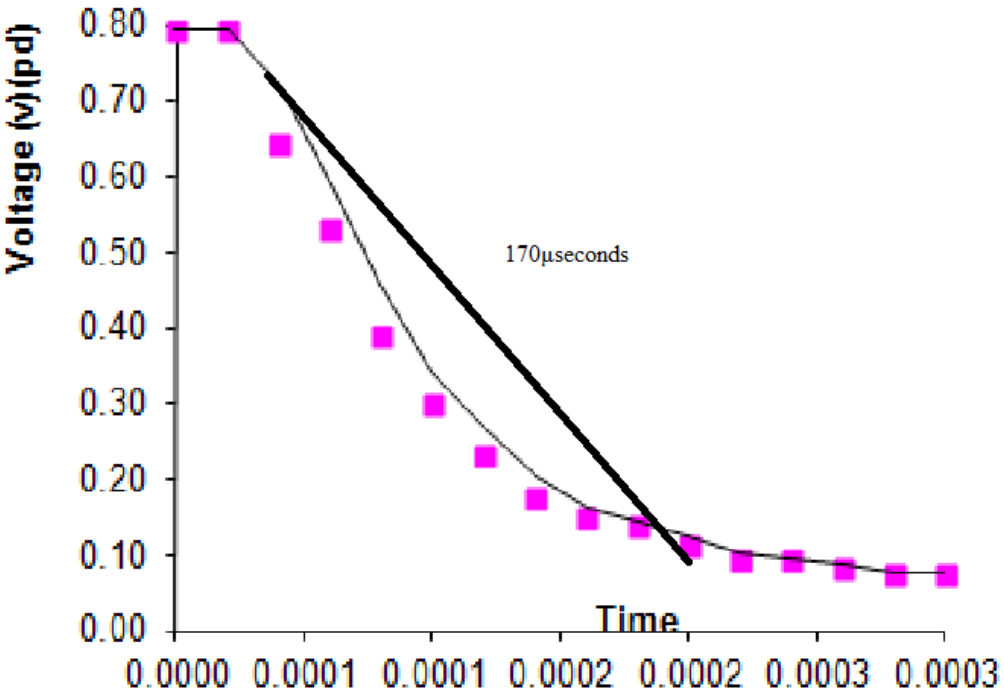

Figure 57 first order switching off time calculation for 20µm electrodes with 8.7µm oil thickness

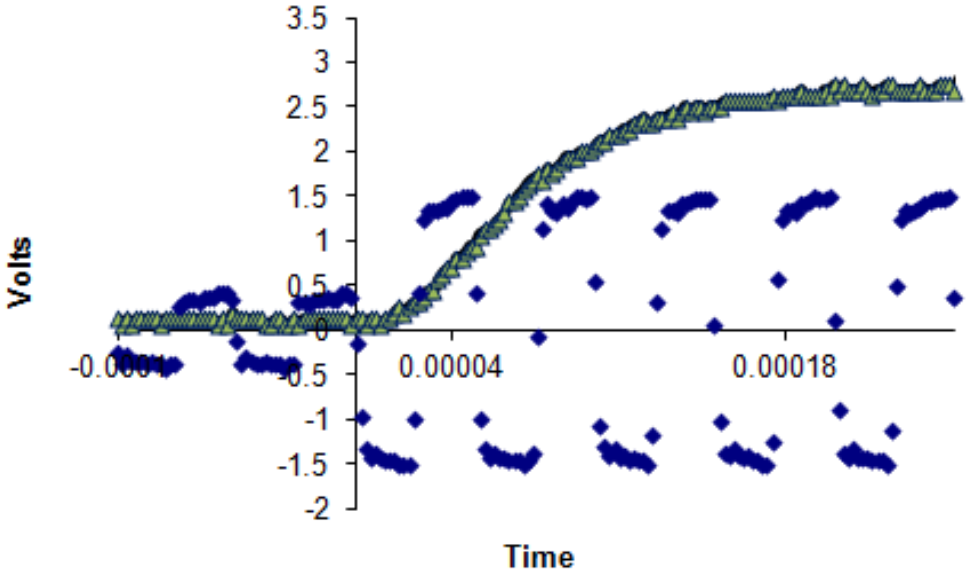

Figure 58 Switching time for first order diffraction spot with 40µm electrodes with 5.8µm oil thickness signal voltage switching on and photo diode switching on (switching time about 140µs).

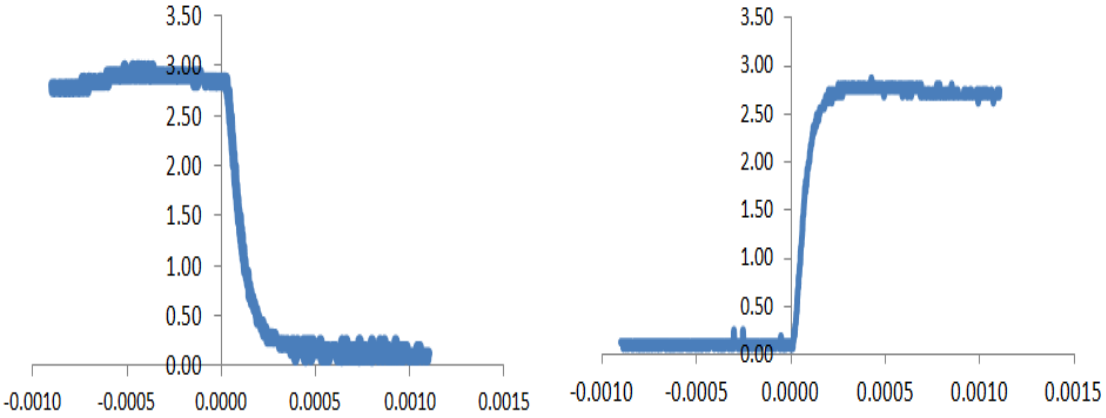

Figure 59 first order diffraction order switching on and switching off for 40µm device.

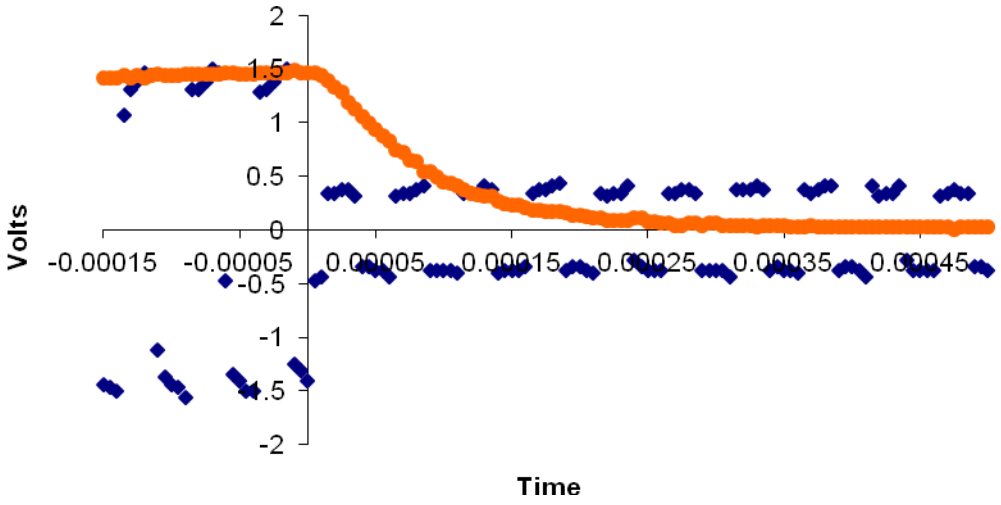

Figure 60 second order switching off for 40µm.

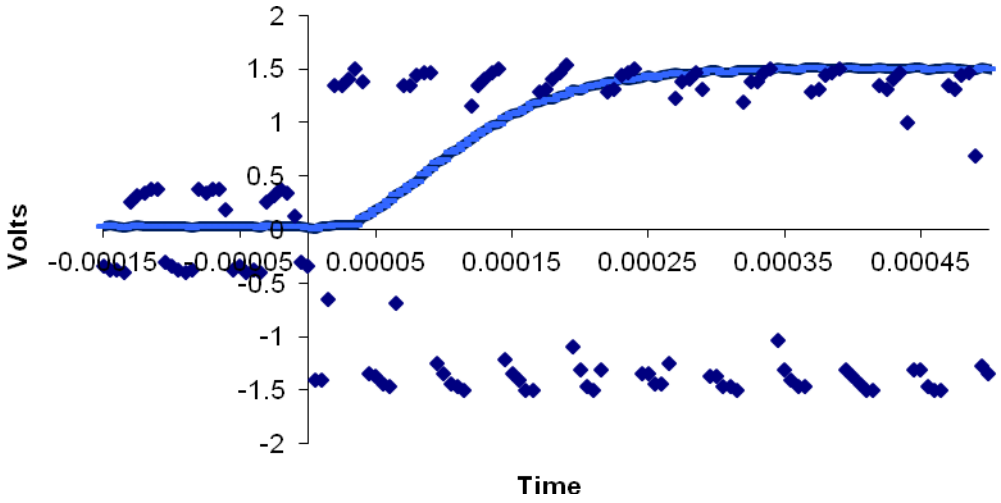

Figure 61second order switching on for 40µm electrodes

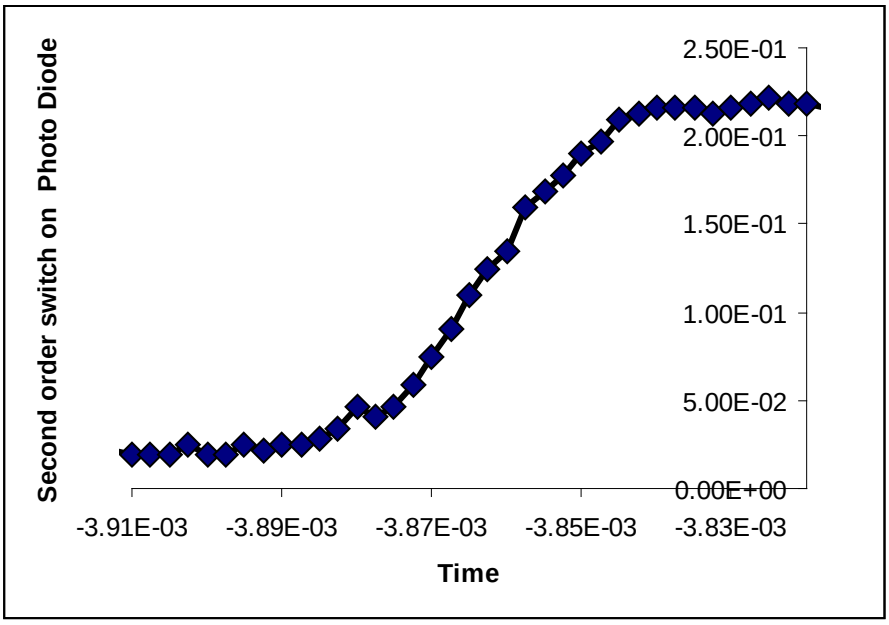

Figure 62 second order diffraction order switching on for 40µ electrodes

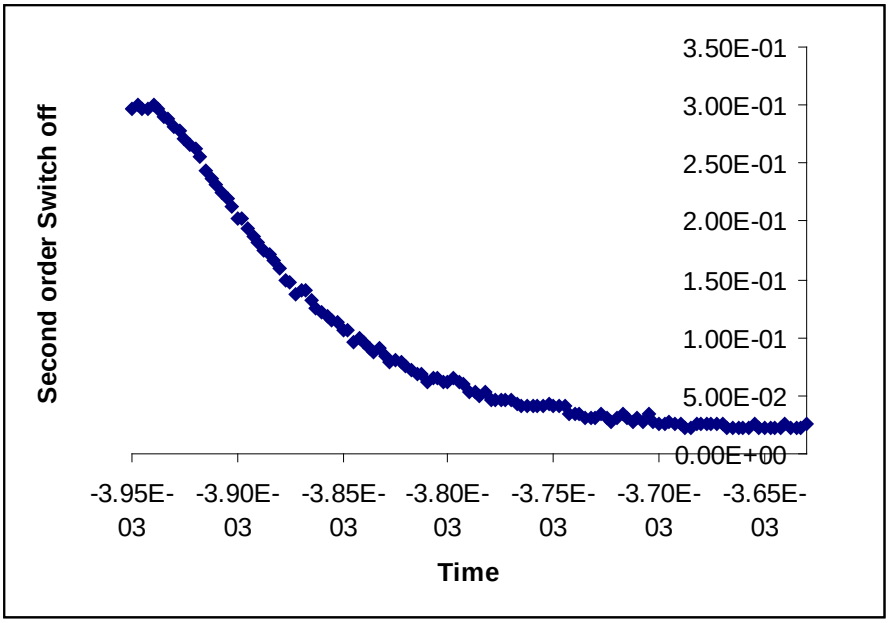

Figure 63 second order diffraction switching off for 40µm device.

Diffraction order	Switch off (µ seconds)	Switch on (µ seconds)
Zero order	140	220
First Order	20	260
Second order	40	230

Table 3 Summary of switching on/off for 40µm device electrodes (80µ pitch) for 8.7µm-5.8µm oil thickness , for zero, First and second orders diffraction spots

Chapter 4 Conclusions and further work

4.1 Introduction

The research work in this thesis was focused on the static and dynamic characterisation of the sinusoidal wrinkle which is produced by using Decanol oil under a non-uniform electrical field. AC voltage is applied to the optical device of electrodes width (20μm, 40μm, 80μm, 120μm and 160μm).

The work in this thesis started to pursue a systematic experimental procedure in order to show the accuracy of the optical device described in chapter 2 for future applications. There were five areas which made those results possible. Firstly, the choice of liquid, secondly, the recipe for producing the IDTs for various gaps between (5μm – 160μm), thirdly, the choice of IDT's surface coating, and lastly, the quality of the data gathering of static and dynamic experiments. The analysis procedure was very important in analysing the experimental data for both static and dynamic experiments. The above areas and experiments were described in chapter 2 and chapter 3.

4.2 The static experiments conclusion

The systematic study of the wrinkle in the static results showed dielectrophoresis forces (L-DEP) have been used to create a static periodic wrinkle with a sinusoidal profile on the surface of a thin layer of 1-Decanol oil. The sinusoidal profile occurs when a voltage V is applied between adjacent co-planar strip electrodes in an interdigitated array onto which the oil film is coated. It has been shown

experimentally that the peak to peak amplitude *A* of the wrinkle scales according to the function of equation 16, for range of oil thickness (between 15 μm and 50 μm) and wrinkle pitches (160μm, 240μm and 320μm) for devices with electrodes widths (40μm, 80μm and 160μm). Thus others oils were used (1-octnol, 2-octnol and paraffin) to verify the model in Appendix A and results were shown in figure 35, figure 38 and figure 39. The model was not accurate for the 1-octnol and 2-octnol in figure 35 and figure 38, because the thickness measurements were taken in three and sometimes four stitched images and especially for the paraffin oil that resulted in having the uncertainty in the model Figure 39. The stitching of those images was done manually see Figure 36 and then errors occurred in the model verification Figure 39. Previous research to model the relationship in Appendix A was failed because measurements did not consider for the first regression of the wrinkle height with V^2 for several measurements at specific thickness and then test the linear relationship in the second regression model.

4.3 Future work of the static experiments

Different types of oils, possibly (1 2-ethanediol), which has a higher surface tension, could be used with the optical device and a further study will be carried out into its characteristics, which relates to how the oil spreads into a thin sinusoidal/nonsinusoidal film with the voltage variation. The future research work into finding different oils will involve the use of the mathematical relationship (equation 16) which was shown to be reliable for predicting the wrinkle amplitude. Another method has shown that solid gratings from NOA65 are possible by using an optical adhesive (e.g. NOA65), which is voltage activated to form an undulation and

then set using UV flood illumination. There is room for systematic work that could be done on the interplay between the setting process and the wrinkle creation dynamics. A dielectric coating could be spread on the top of the set NOA65 gratings to help form the sinusoidal gratings.

4.4 The dynamic experiments

In those experiments devices with 20 μm and 40 μm electrodes width were used to examine the switching time response of the photo LED detector, and to establish the Bessel function relationship between the zero, first and second. The results need to be studied and classified in terms of the effect of different oil parameters, switching time with the wrinkle signal voltage, thickness of oil at those measurements and also relate it to the sensitivity of the photo diode on the switching time. As it was shown in chapter 3 the sensitivity of the detector increases the switching time and reduces, this effect needs to be studied. The future of these experiments will be by adding more photo detectors (3 detectors for zero, first and second orders) and better 4 channels oscilloscope is needed, as is shown in Figure 64 initial results . The preliminary experiment was tried and used of three photo diodes DET36A and four channels oscilloscope have provided fast clear results on the zero, first and second diffraction spots and the signal voltage. This will make the drop of oil last longer before evaporates because less time is needed to record the results and change the position of a single detector that was used in chapter 3.

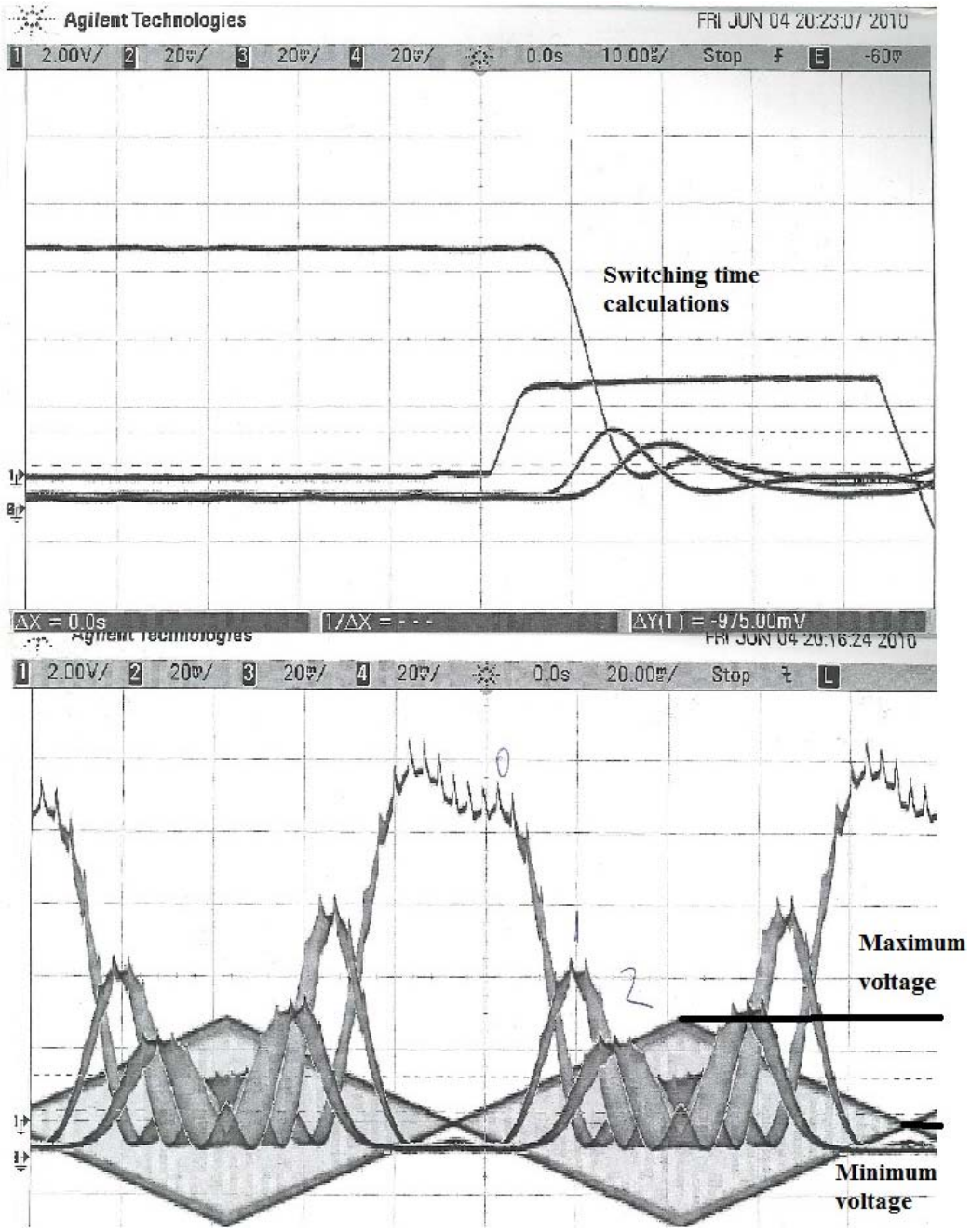

Figure 64 Dynamic experiments with 4 channels oscilloscope and three photo detectors initial results

4.5 Future work on the IDT

The current IDT is made by using the photolithography process in chapter 2, to produce the wanted IDT structure from ITO coated glass with a mask. The mask has been designed to have equal periodic changes of electrode widths/gaps. The width of

electrodes (W_{elect}) is the same as the width of the gap between the electrodes (W_{gap}) as shown in the table below.

W_{elect}=40 µm W_{gap}=40 µm	W_{elect}=20 µm W_{gap}=20 µm	W_{elect}=160 µm W_{gap}=160 µm	W_{elect}=200 µm W_{gap}=200 µm
W_{elect}=5 µm W_{gap}=5 µm	W_{elect}=10 µm W_{gap}=10 µm	W_{elect}=120 µm W_{gap}=120 µm	W_{elect}=80 µm W_{gap}=80 µm

It is proposed to make the electrodes wider with a 3/1 ratio, as shown in the table below.

W_{elect}=60 µm Wgap=20 µm	W_{elect}=30 µm W_{gap}=10 µm	W_{elect}=240 µm W_{gap}=80 µm	W_{elect}=300 µm W_{gap}=100 µm
W_{elect}=7.5µm W_{gap}=2.5µm	W_{elect}=15µm W_{gap}=5µm	W_{elect}=180µm W_{gap}=60µm	W_{elect}=120µm W_{gap}=40µm

Another idea is to add a set of electrodes with a certain ratio between the gaps as shown in the table below:

W_{elect}=40 µm Wgap=10 µm W_{2elect}=20 µm W_{2gap}=10 µm	W_{elect}=20 µm W_{gap}=5 µm W_{2elect}=10 µm W_{2gap}=5 µm	W_{elect}=160 µm W_{gap}=40 µm W_2elect=80 µm W_{2gap}=40 µm	W_{elect}=200 µm W_{gap}=50 µm W_{2elect}=100 µm W_{2gap}=50 µm
W_{elect}=40 µm W_{gap}=40 µm	W_{elect}=20 µm W_{gap}=20 µm	W_{elect}=120 µm W_{gap}=30 µm W_{2elect}=60 µm W_{2gap}=30 µm	W_{elect}=80 µm W_{gap}=20 µm W_{2elect}=40 µm W_{2gap}=20 µm

The adding of additional electrode regions will be used to control the spread of the oil film and to control the shape of the wrinkle. The extra electrode regions could be used in droplet separation proposal as discussed in section 4.6. There is already a mask with different spacing in the thin film lab which could be used in future

experiments. Another possibility is to have a different electrodes shape. A photolithography mask is needed to be designed for this task.

There is another method of producing a highly non uniform electric field by using carbon nanofibres as was reporteded by (Teo, 2002). The carbon nanofibres were prepared using plasma-enhanced chemical vapour deposition of acetylene and ammonia gases in the presence of a nickel catalyst. It was reported that the patterned array of individual vertically aligned nanofibres had the most desirable field emission characteristics by using arrays of conducting shapes e.g. an array of carbon nanotubes (Teo, 2002). This method is a complicated and requires special expertise, equipment and labs to align the carbon nanotubes and requires an outside collaborator to help in this field. It will open a new dimension in the use of the optical device.

4.6 Further work on manipulation and spreading of oil droplet

There is another method of producing a highly non uniform electric field by using carbon nanofibres as was reported by (Teo, 2002). The carbon nanofibres were prepared using plasma-enhanced chemical vapour deposition of acetylene and ammonia gases in the presence of a nickel catalyst. It was reported that the patterned array of individual vertically aligned nanofibres had the most desirable field emission characteristics by using arrays of conducting shapes e.g. an array of carbon nanotubes (Teo, 2002).

4.7 Single/two fluid droplet segregation research

Depending upon the progress within the previous sections, should time be available, there is an important investigation that will examine the use of the optical device in segregation of droplet(s) and the factors which affect the movement of the droplet(s). The factors considered are the AC voltage and the electric field, which is generated to move a single droplet towards areas of high field intensity. The investigation will look at the effects of lowering the surface tension on the segregation of the single droplet. The research will investigate the ways in which the interaction between the two droplets and the solid surface of the device is affected. The research will also consider using detergents, wetting agents and emulsions to increase or decrease the interaction. The electrodes geometry of the device will be investigated and the effects on the above parameters. Internally, a square and a circular shape will be incorporated in the mask design. The profile of the highly non uniform fringing electric fields can be engineered to some extent by changing the thickness profile of the dielectric in a systematic manner within each period, e.g. by producing shaped dielectric surface profiles, or an architecture that will allow the creation of solid surface grating structures (e.g. a grating switched in/out by microfluidic movement to give refractive index mis/matching). This engineered non-uniform field has been shown in the work of Professor Velev from the University of North Carolina, as shown in figure 65.

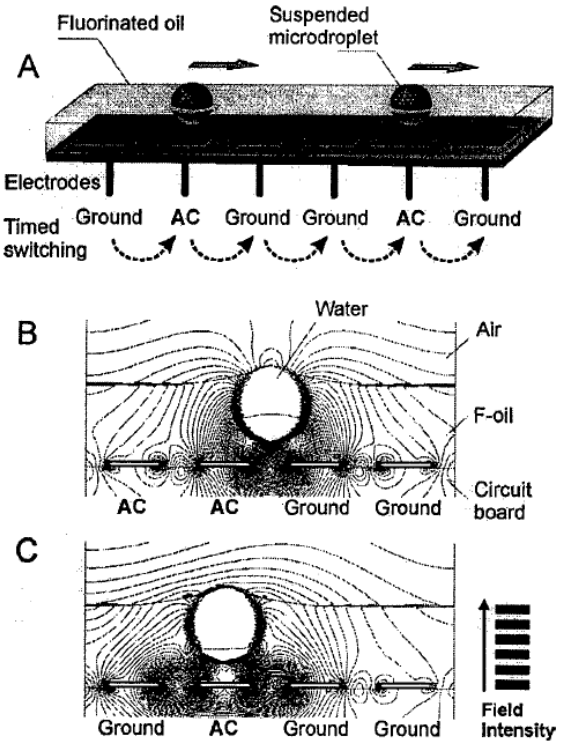

Figure 65 Schematics of the operation of the dielectrophoretic segregation of droplets using the non-uniform field intensity

(Courtesy to Professor Velev of North Carolina state University, Raleigh 5/12/2004)

4.8 Future Tasks

The dynamic experimental will set up with hexadecane oil that is known to generate a non-sinusoidal wrinkle will replace the Decanol oil experiment and a new procedure for non-sinusoidal data to be implemented. The other tasks for the non-sinusoidal wrinkle that will be investigated for the following parameters in the optical device with hexadecane oil are:-

- Accurate surface tension
- Accurate dielectric constants
- Accurate viscosity and shear modules
- Accurate distance between the electrodes and electrodes width
- Patterned structures electrodes as compared to the existence electrodes

Appendix A

(Modelling relationship of oil surface undulation)

(This mathematical derivation was done by Professor Carl Brown and Professor G McHale, Nottingham Trent University)

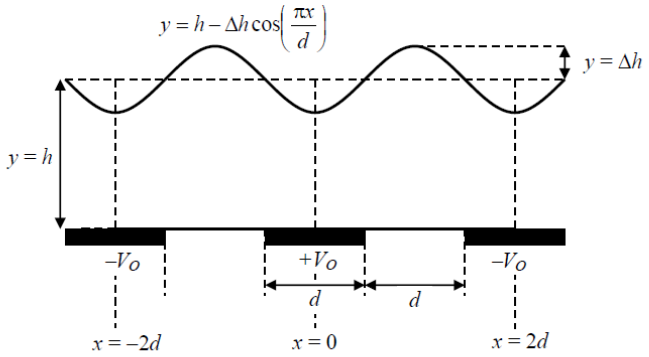

Dielectric energy

Voltage profile [H. Morgan, J. Phys. D. 34, 1553 (2001)] as a sum of Fourier components :

$$V(x,y) = \sum_{n=1}^{\infty} A_n \cos(k_n x)\exp(-k_n y)$$

where $k_n = \frac{(2m+1)\pi}{2d}$ and $A_n = \frac{16V_o}{\pi^2(2m+1)^2}\cos\left[(2m+1)\frac{\pi}{4}\right]$

Calculate the electric field profile :

$$E(x,y) = -\nabla V = -\begin{pmatrix} \partial V/\partial x \\ \partial V/\partial y \\ \partial V/\partial z \end{pmatrix} = \begin{pmatrix} \sum_{n=1}^{\infty} A_n k_n \sin(k_n x)\exp(-k_n y) \\ \sum_{n=1}^{\infty} A_n k_n \cos(k_n x)\exp(-k_n y) \\ 0 \end{pmatrix}$$

Calculate the energy :

$$W = \frac{1}{2}\mathbf{D}\cdot\mathbf{E} = \frac{1}{2}\varepsilon\mathbf{E}\cdot\mathbf{E}$$

$$2W = \varepsilon\left[\left(\sum_{n=1}^{\infty} A_n k_n \sin(k_n x)\exp(-k_n y)\right)^2 + \left(\sum_{n=1}^{\infty} A_n k_n \cos(k_n x)\exp(-k_n y)\right)^2\right]$$

$$2W = \varepsilon\left[\begin{array}{l}\left(A_1 k_1 \sin(k_1 x)\exp(-k_1 y) + A_2 k_2 \sin(k_2 x)\exp(-k_2 y) + \cdots\right)^2 \\ + \left(A_1 k_1 \cos(k_1 x)\exp(-k_1 y) + A_2 k_2 \cos(k_2 x)\exp(-k_2 y) + \cdots\right)^2\end{array}\right]$$

Expansion to 3rd order :

$$\begin{aligned}2W = \varepsilon[&A_1^2 k_1^2 \sin^2(k_1 x)\exp(-2k_1 y) + A_2^2 k_2^2 \sin^2(k_2 x)\exp(-2k_2 y) + \cdots \\ &+ 2A_1 k_1 A_2 k_2 \sin(k_1 x)\sin(k_2 x)\exp(-(k_1 + k_2)y) + \\ &+ 2A_1 k_1 A_3 k_3 \sin(k_1 x)\sin(k_3 x)\exp(-(k_1 + k_3)y) + \cdots \\ &+ A_1^2 k_1^2 \cos^2(k_1 x)\exp(-2k_1 y) + A_2^2 k_2^2 \cos^2(k_2 x)\exp(-2k_2 y) + \cdots \\ &+ 2A_1 k_1 A_2 k_2 \cos(k_1 x)\cos(k_2 x)\exp(-(k_1 + k_2)y) + \\ &+ 2A_1 k_1 A_3 k_3 \cos(k_1 x)\cos(k_3 x)\exp(-(k_1 + k_3)y) + \cdots]\end{aligned}$$

Trigonometrical identity : $\cos^2 A + \sin^2 A = 1$

$$\begin{aligned}2W = \varepsilon[&A_1^2 k_1^2 \exp(-2k_1 y) + A_2^2 k_2^2 \exp(-2k_2 y) + \cdots \\ &+ 2A_1 k_1 A_2 k_2 \sin(k_1 x)\sin(k_2 x)\exp(-(k_1 + k_2)y) + \\ &+ 2A_1 k_1 A_3 k_3 \sin(k_1 x)\sin(k_3 x)\exp(-(k_1 + k_3)y) + \cdots \\ &+ 2A_1 k_1 A_2 k_2 \cos(k_1 x)\cos(k_2 x)\exp(-(k_1 + k_2)y) + \\ &+ 2A_1 k_1 A_3 k_3 \cos(k_1 x)\cos(k_3 x)\exp(-(k_1 + k_3)y) + \cdots]\end{aligned}$$

where $k_1 = \dfrac{\pi}{2d}$, $A_1 = \dfrac{16V_o}{\pi^2}\cos\left[\dfrac{\pi}{4}\right] = \dfrac{16V_o}{\sqrt{2}\pi^2}$

$$k_2 = \frac{3\pi}{2d},\ A_2 = \frac{16V_o}{9\pi^2}\cos\left[\frac{3\pi}{4}\right] = -\frac{16V_o}{9\sqrt{2}\pi^2}$$

$$k_3 = \frac{5\pi}{2d},\ A_3 = \frac{16V_o}{25\pi^2}\cos\left[\frac{5\pi}{4}\right] = -\frac{16V_o}{25\sqrt{2}\pi^2}$$

Orders of terms in the Fourier expansion :

1st order $\exp(-2k_1 y) = \exp\left(-\dfrac{\pi}{d}\right)$

2nd order $\exp(-(k_1 + k_2)y) = \exp\left(-\dfrac{2\pi}{d}\right)$

3rd order $\exp(-2k_2 y) = \exp\left(-\dfrac{3\pi}{d}\right)$, $\exp(-(k_1 + k_3)y) = \exp\left(-\dfrac{3\pi}{d}\right)$

Keep terms up to second order only :

$$\begin{aligned}2W = \varepsilon[&A_1^2 k_1^2 \exp(-2k_1 y) + 2A_1 k_1 A_2 k_2 \sin(k_1 x)\sin(k_2 x)\exp(-(k_1 + k_2)y) + \\ &+ 2A_1 k_1 A_2 k_2 \cos(k_1 x)\cos(k_2 x)\exp(-(k_1 + k_2)y)]\end{aligned}$$

$$W = \frac{16\varepsilon V_o^2}{d^2\pi^2}[\exp\left(-\frac{\pi y}{d}\right) - \frac{2}{3}\sin\left(\frac{\pi x}{2d}\right)\sin\left(\frac{3\pi x}{2d}\right)\exp\left(-\frac{2\pi y}{d}\right) +$$
$$-\frac{2}{3}\cos\left(\frac{\pi x}{2d}\right)\cos\left(\frac{3\pi x}{2d}\right)\exp\left(-\frac{2\pi y}{d}\right)]$$

Trigonometrical identities : $\sin 3A = 3\sin A - 4\sin^3 A$
$\cos 3A = 4\cos^3 A - 3\cos A$

$$W = \frac{16\varepsilon V_o^2}{d^2\pi^2}\left[\exp\left(-\frac{\pi y}{d}\right) - \frac{2}{3}\left[3\sin^2\left(\frac{\pi x}{2d}\right) - 4\sin^4\left(\frac{\pi x}{2d}\right) + 4\cos^4\left(\frac{\pi x}{2d}\right) - 3\cos^2\left(\frac{\pi x}{2d}\right)\right]\exp\left(-\frac{2\pi y}{d}\right)\right]$$

Difference of two squares : $\cos^4 A - \sin^4 A = (\cos^2 A - \sin^2 A)(\cos^2 A + \sin^2 A)$

Trigonometrical identities :
$\cos^2 A + \sin^2 A = 1$
$\cos 2A = \cos^2 A - \sin^2 A$

$$W = \frac{16\varepsilon V_o^2}{d^2\pi^2}\left[\exp\left(-\frac{\pi y}{d}\right) - \frac{2}{3}\cos\left(\frac{\pi x}{d}\right)\exp\left(-\frac{2\pi y}{d}\right)\right]$$

Find electrical energy in the volume :

$$W_T = \frac{16l\varepsilon V_o^2}{d^2\pi^2}\int_{-2d}^{+2d}\int_0^{h-\Delta h\cos(kx)}\left[\exp\left(-\frac{\pi y}{d}\right) - \frac{2}{3}\cos\left(\frac{\pi x}{d}\right)\exp\left(-\frac{2\pi y}{d}\right)\right]dydx$$

$$W_T = -\frac{16l\varepsilon V_o^2}{d\pi^3}\int_{-2d}^{+2d}\left[\exp\left(-\frac{\pi y}{d}\right) - \frac{1}{3}\cos\left(\frac{\pi x}{d}\right)\exp\left(-\frac{2\pi y}{d}\right)\right]_0^{h-\Delta h\cos(kx)}dx$$

$$W_T = -\frac{16l\varepsilon V_o^2}{d\pi^3}\int_{-2d}^{+2d}\left[\begin{array}{l}\exp\left(-\frac{\pi(h-\Delta h\cos(kx))}{d}\right) - 1 \\ -\frac{1}{3}\exp\left(-\frac{2\pi(h-\Delta h\cos(kx))}{d}\right)\cos\left(\frac{\pi x}{d}\right) + \frac{1}{3}\cos\left(\frac{\pi x}{d}\right)\end{array}\right]dx$$

$$W_T = -\frac{16l\varepsilon V_o^2}{d\pi^3}\int_{-2d}^{+2d}\left[\begin{array}{l}\exp\left(-\frac{\pi h}{d}\right)\exp\left(\frac{\pi\Delta h\cos(kx))}{d}\right) - 1 \\ -\frac{1}{3}\exp\left(-\frac{2\pi h}{d}\right)\exp\left(\frac{2\pi\Delta h\cos(kx)}{d}\right)\cos\left(\frac{\pi x}{d}\right) + \frac{1}{3}\cos\left(\frac{\pi x}{d}\right)\end{array}\right]dx$$

Series expansion for small $\Delta h << d/2\pi$: $\exp(x) = 1 + x + \frac{x^2}{2} + \frac{x^3}{6} + \cdots \approx 1 + x$

$$W_T = -\frac{16 l \varepsilon V_o^2}{d \pi^3} \int_{-2d}^{+2d} \left[\begin{array}{l} \exp\left(-\frac{\pi h}{d}\right)\left(1+\frac{\pi \Delta h \cos(kx))}{d}\right)-1 \\ -\frac{1}{3}\exp\left(-\frac{2\pi h}{d}\right)\left(1+\frac{2\pi \Delta h \cos(kx)}{d}\right)\cos\left(\frac{\pi x}{d}\right)+\frac{1}{3}\cos\left(\frac{\pi x}{d}\right) \end{array} \right] dx$$

Let $k = \frac{\pi}{d}$, as shown by the geometry earlier

$$W_T = -\frac{16 l \varepsilon V_o^2}{d^2 \pi^3} \int_{-2d}^{+2d} \left[\begin{array}{l} \exp\left(-\frac{\pi h}{d}\right)\left(d+\pi \Delta h \cos\left(\frac{\pi x}{d}\right)\right)-d \\ -\frac{1}{3}\exp\left(-\frac{2\pi h}{d}\right)\left(d\cos\left(\frac{\pi x}{d}\right)+2\pi \Delta h \cos^2\left(\frac{\pi x}{d}\right)\right)+\frac{d}{3}\cos\left(\frac{\pi x}{d}\right) \end{array} \right] dx$$

$$W_T = -\frac{16 l \varepsilon V_o^2}{d^2 \pi^3} \left[\begin{array}{l} \exp\left(-\frac{\pi h}{d}\right)\left(xd+d\Delta h \sin\left(\frac{\pi x}{d}\right)\right)-xd \\ -\frac{1}{3}\exp\left(-\frac{2\pi h}{d}\right)\left(\frac{d^2}{\pi}\sin\left(\frac{\pi x}{d}\right)+2d\Delta h\left(\frac{\pi x}{2d}+\frac{1}{4}\sin\left(\frac{2\pi x}{d}\right)\right)\right) \\ +\frac{d^2}{3\pi}\sin\left(\frac{\pi x}{d}\right) \end{array} \right]_{-2d}^{2d}$$

$$W_T = -\frac{16 l \varepsilon V_o^2}{d^2 \pi^3} \left[4d^2 \left[\exp\left(-\frac{\pi h}{d}\right)-1 \right] - \frac{4d\pi \Delta h}{3} \exp\left(-\frac{2\pi h}{d}\right) \right]$$

$$W_T = -\frac{64 l \varepsilon V_o^2}{\pi^3} \left[\left[\exp\left(-\frac{\pi h}{d}\right)-1 \right] - \frac{\pi \Delta h}{3d} \exp\left(-\frac{2\pi h}{d}\right) \right]$$

<u>Interfacial energy</u>

Length of a sinusoidal interface (following Glen's analysis from July 2004) :

$$y = h - \Delta h \cos\left(\frac{\pi x}{d}\right)$$

$$L = \int_{-2d}^{+2d} \left[1+\left(\frac{dy}{dx}\right)^2 \right]^{1/2} dx = \int_{-2d}^{2d} \left[1+\left(\frac{\pi \Delta h}{d}\right)^2 \sin^2\left(\frac{\pi x}{d}\right) \right]^{1/2} dx$$

Write integral in a standard form using the substitution $u = \pi x / d$.

$$L = \left(\frac{d}{\pi}\right) \int_{-2\pi}^{2\pi} \left[1+\left(\frac{\pi \Delta h}{d}\right)^2 \sin^2 u \right]^{1/2} du = \left(\frac{8d}{\pi}\right) \int_0^{\pi/2} \left[1 - m \sin^2 u \right]^{1/2} du \quad \text{and} \quad m = -\left(\frac{\pi \Delta h}{d}\right)^2$$

Incomplete elliptical integral of the second kind : if $|m| < 1$, this integral can be approximated by the series expansion :

$$E(m) = \int_0^{\pi/2} \left[1 - m\sin^2\theta\right]^{1/2} d\theta, \quad E(m) \approx \frac{\pi}{2}\left[1 - \left(\frac{1}{2}\right)^2 m - \left(\frac{1\cdot 3}{2\cdot 4}\right)^2 \frac{m^2}{3} + \ldots\right] \qquad |m| < 1$$

$$L = \frac{\pi}{2}\left(\frac{8d}{\pi}\right)\left[1 + \left(\frac{1}{2}\right)^2\left(\frac{\pi\Delta h}{d}\right)^2 - \left(\frac{3}{24}\right)^2\left(\frac{\pi\Delta h}{d}\right)^4 + \ldots\right] \approx 4d\left[1 + \left(\frac{\pi\Delta h}{2d}\right)^2\right]$$

Length of a sinusoidal interface (new approach, do a binomial expansion first) :

$$\left[1 + \left(\frac{dy}{dx}\right)^2\right]^{1/2} \approx 1 + \frac{1}{2}\left(\frac{dy}{dx}\right)^2, \quad y = h - \Delta h\cos\left(\frac{\pi x}{d}\right)$$

$$l = \int_{-2d}^{+2d}\left[1 + \frac{1}{2}\left(\frac{dy}{dx}\right)^2\right]dx = \int_{-2d}^{2d}\left[1 + \left(\frac{\pi^2\Delta h^2}{2d^2}\right)\sin^2\left(\frac{\pi x}{d}\right)\right]dx$$

Trigonometrical identity : $\sin^2 A = \frac{1}{2} - \frac{1}{2}\cos 2A$

$$l = \int_{-2d}^{2d}\left[1 + \left(\frac{\pi\Delta h}{2d}\right)^2 - \left(\frac{\pi\Delta h}{2d}\right)^2\cos\left(\frac{2\pi x}{d}\right)\right]dx$$

$$l = \left[x + \left(\frac{\pi\Delta h}{2d}\right)^2 x - \left(\frac{d}{2\pi}\right)\left(\frac{\pi\Delta h}{2d}\right)^2\sin\left(\frac{2\pi x}{d}\right)\right]_{-2d}^{2d}$$

$l = 4d\left[1 + \left(\frac{\pi\Delta h}{2d}\right)^2\right]$ reassuringly, gives same answer as above to first order

Interfacial energy $W_I = 4dl\gamma\left[1 + \left(\frac{\pi\Delta h}{2d}\right)^2\right]$

<u>Equating energies</u>

$$W = W_I - W_T = 4dl\gamma\left[1 + \left(\frac{\pi\Delta h}{2d}\right)^2\right] + \frac{64l\varepsilon V_o^2}{\pi^3}\left[\left[\exp\left(-\frac{\pi h}{d}\right) - 1\right] - \frac{\pi\Delta h}{3d}\exp\left(-\frac{2\pi h}{d}\right)\right]$$

$$\frac{\partial W}{\partial \Delta h} = 8dl\gamma\left(\frac{\pi}{2d}\right)^2\Delta h - \frac{64l\varepsilon V_o^2}{3d\pi^2}\exp\left(-\frac{2\pi h}{d}\right)$$

for minimum energy set $\frac{\partial W}{\partial \Delta h} = 0$

$$\Delta h = \frac{32\varepsilon V_o^2}{3\gamma\pi^4}\exp\left(-\frac{2\pi h}{d}\right)$$

Correct dimensionally :

d	metre
ε	Farad / metre
γ	Joule / metre^2
V	volts ≡ Joule$^{1/2}$ Farad$^{-1/2}$ so volts^2 ≡ Joule / Farad

Appendix B

Publications of the Author and joint work

Amplitude scaling of a static wrinkle at an oil-air interface created by dielectrophoresis forces, Brown, C. V.; Al-Shabib, W.; Wells, G. G.; McHale, G.; Newton, M. I. , Applied Physics Letters, Volume 97, Issue 24, id. 242904 (3 pages) (2010).

Fast reconfigurable liquid optical interface, Carl V. Brown, Gary G. Wells,Wamid Al-Shabib, Glen McHale, Michael I. Newton, Nottingham Trent Univ. (United Kingdom) [7716-15], Conferences: 12-16 April 2010 SPIE Photonics, Brussels, Belgium

Voltage programmable liquid-based diffraction grating
Wamid Al-Shabib, C.V. Brown, G.G.Wells, G.McHale, and M.I. Newton, School of Science and Technology, Nottingham Trent University, Nottingham NG11 8NS.

References

ARUMUGAM, P.U., 2007. Dielectrophoretic Trapping of Single Bacteria at Carbon Nanofiber Nanoelectrode Arrays. *Journal of Physical Chemistry,* 111 (49), 12772-12777.

AUBRY, N., SINGH and P, 2006. Control of electrostatic particle-particle interactions in dielectrophoresis. *EPL (Europhysics Letters),* 74 (4).

BALLANTYNE, G. and HOLTHAM, P., 2010. Application of dielectrophoresis for the separation of minerals. *Minerals Engineering,* 23 (4), 350-358.

BARDEN, S.C., 1999.
Tunable Gratings: Imaging the Universe in 3-D with Volume-Phase Holographic Gratings. *In:* .

BARNES, G. and GENTLE, I., 2005. *Interfacial Science: An Introduction.* Oxford University Press.

BLOOM, D., 1997. The grating light valve: Revolutionizing display technology. *In: PROJECTION DISPLAYS III,* SPIE - INT SOC OPTICAL ENGINEERING, pp. 165-171.

BROWN, C.V., et al., 2009. Voltage-programmable liquid optical interface. *Nature Photonics,* 3 (7), 403-405.

BROWN, C., NEWTON, M. and MCHALE, G., 2006. *Switchable Diffraction Grating.* GB2422680A.

CROSSLAND, W., et al., 2004. Liquid crystals in Telecommunications Systems. *Molecular Crystals and Liquid Crystals,* 413, 2499-2519.

CUI, Z., et al., 2010. Space-resolved vacuum ultraviolet spectrometer system for edge impurity and temperature profile measurement in HL-2A. *Review of Scientific Instruments,* 81 (4).

FERRINI, R.E.A., 2008. Hybrid inorganic-organic photonic devices. *In: European Optical Society Annual Meeting 2008, Paris, 29-October 2, 2008.* Paris: .

GANG YE, CANQIANG YANG, XIAOGONG WANG, 2010. Sensing Diffraction Gratings of Antigen-Responsive Hydrogel for Human Immunoglobulin-G Detection. *Macromolecular Rapid Communications,* 31, 1332-1336.

GOODMAN, J.W., 2005. *Introduction to Fourier Optics.* Roberts.

GUNJI, M., JOHNES, T.B, 2000. Dielectrophoretic Microfluidic Devices. *In:* pp. 78-87.

HECHT, E., 2002. *Optics.* Addison Wesley.

HEIKENFELD, J. and STECKL, A., 2005. High-transmission electrowetting light valves. *Applied Physics Letters,* 86 (15).

HEIKENFELD, J., et al., 2008. Flat electrowetting optics and displays - art. no. 688705. *Proceedings of SPIE--the International Society for Optical Engineering,* 6887, 88705-88705.

HEIKKILA, N., et al., 2008. Design and Analysis of Compact Spectrometer for Illumination Recognition. *Japanese Journal of Applied Physics,* 47 (8), 6695-6698.

HIROTA, Y., HAKODA, M. and WAKIZAKA, Y., 2010. Separation characteristics of animal cells using a dielectrophoretic filter. *Bioprocess and Biosystems Engineering,* 33 (5), 607-612.

JIE, Z.A.Y.,Z., et al., 2009. Experiments of a Grating Light Modulator for Projection Display Applications. *Applied Optics,* 48 (9), 1675-1681.

KALER, K., 2010. Liquid dielectrophoresis and surface microfluidics. *In:* .

LEE, M.S.L., ET AL, 2003. Transmission blazed-binary grating for visible light operation: performances and interferometric characterization. *Journal of Optics A: Pure and Applied Optics,* 5 (5).

LEE, B., et al., 2004. Applications of holographic devices for optical communications. *Proceedings of SPIE--the International Society for Optical Engineering,* 5560, 105-116.

LEE, B., CHOI, W. and NA, J., 2009. *Simultaneous refractive indices and thicknesses measurements in non-live materials using optical coherence tomography.* IEEE: .

LEE, M., et al., 2003. Transmission blazed-binary gratings for visible light operation: performances and interferometric characterization. *Journal of Optics A-Pure and Applied Optics,* 5 (5), S244-S249.

LISCIDINI, M., 2009. Enhancing Light-Matter Interaction via Bloch Surface Waves for Biosensing Applications. *In:* pp. 472-475.

LORRAIN, P. and CORSON, D., 1988. *Electromagnetic Fields and Waves.* W H Freeman and Company.

LOWANS, B.S., 1994. *Applications of spatial light modulators in optical information processing. [electronic resource].* Queen's University of Belfast.

MATSUMOTO, S., et al., 2006. Phase grating using a ferroelectric liquid-crystal mixture with a photocurable liquid crystal. *Journal of Applied Physics,* 99 (11).

MCCAMLEY, M.K., et al., 2009. Detection of alignment changes at the open surface of a confined nematic liquid crystal sensor. *Journal of Applied Physics,* 105 (12).

MEVEL, Y., et al., 2003. Characterisations of a 2x2 optical switch using an acousto-optic cell with phased array transducers. *Proceedings of SPIE--the International Society for Optical Engineering,* 4946, 192-200.

MOHARAM, M.G., ET AL, 1980. CRITERIA FOR RAMAN-NATH REGIME DIFFRACTION BY PHASE GRATINGS. *OPTICS COMMUNICATIONS,* 32 (1), 19-23.

PETHIG, R., 1996. Dielectrophoresis: Using inhomogeneous AC electrical fields to separate and manipulate cells. *Critical Reviews in Biotechnology,* 16 (4), 331-348.

PHILIPIS NEWS, 2004. *Philips shows functional, large-scale demonstrator of its electrowetting-based electronic-paper technology* [online]. IOP. Available at: http://www.physorg.com/news285.html.

POHL, H., 1978. *Dielectrophoresis.* Cambridge Monographs on Physics.

REGTMEIE, J.E.A., 2010. Dielectrophoretic Trapping and Polarizability of DNA: The Role of Spatial Conformation. *American Chemical Society,* (10.1021/ac1005475).

RESLER, D., et al., 1996. High-efficiency liquid-crystal optical phased-array beam steering. *Optics Letters,* 21 (9), 689-691.

REZA, R., et al., 2010. Sorting ZnO particles of different shapes with low frequency AC electric fields. *Materials Letters,* .

SCHEFFER, T. and NEHRING, J., 1984. A New, Highly Multiplexable Liquid-Crystal Display. *Applied Physics Letters,* 45 (10), 1021-1023.

SENTURIA, S., et al., 2005. Programmable diffraction gratings and their uses in displays, spectroscopy, and communications. *Journal of Microlithography, Microfabrication, and Microsystems,* 4 (4).

SHAOULOV, I. V, ET AL, 2002. Compact relay lenses using microlenslet arrays. *In: SPIE International Optical Design Conference, San Francisco, California, USA, 22-27 January 2002.* SPIE, pp. 74-79.

SONG, M., 2010. Thickness and roughness measurement using a reflective digital holographic microscope *In: SPIE, USA, 26 March 2010.* USA: SPIE, pp. 1100-1120.

TANONE, A., et al., 1994. Optical Beam-steering Using A Liquid-Crystal Television Panel. *Microwave and Optical Technology Letters,* 7 (6), 285-289.

TEO, K. B. K. ET AL, 2002. Field emission from dense, sparse, and patterned arrays of carbon nanofibers. *APPLIED PHYSICS LETTERS,* 18 (11), 2011-2013.

TOCNAYE, D.L., 2004. Engineering liquid crystals for optimal uses in optical communication systems. *Liquid Crystals,* 31 (2), 241-269.

VAMSEE K. PAMULA MICHAEL G. POLLACK RICHARD B. FAIR PHILIP Y. PAIK HONG REN, 2009. *Electrowettings Patent application title: Methods for Manipulating Droplets by Electrowetting-Based Techniques.* 20090260988.

WEI, H., et al., 2010. Transmissive beam steering through electrowetting microprism arrays. *Optics Communications,* 283 (6), 1174-1181.

WELCH, D., 2010. Thickness Measurements Using Laser Triangulation. *Sensors,* 1 (4), 10-15.

WELLS, G.G., 2009. *Voltage programmable liquid optical devices. PhD. Nottingham Trent University.* PhD., Nottingham Trent University.

YOSHIMURA, T.E.A., January 20th 2011. *Thin-Film Organic Photonics; Molecular Layer Deposition and Applications.* eBook ed. http://www.taylorandfrancis.com/books/details/9781439819739/: Optics and Photonics.

YU DU GUANGYA ET AL, 2009. A 2-DOF Circular-Resonator-Driven In-Plane Vibratory Grating Laser Scanne**r** . *Journal of Micromechanics and Microengineering,* 18 (4), 892-904.